Journal of Experimental Botany, Vol. 66, No. 19 pp. 5929–5943, 2015
doi:10.1093/jxb/erv302 Advance Access publication 1 July 2015

RESEARCH PAPER

Functional characterization of the homeodomain leucine zipper I transcription factor AtHB13 reveals a crucial role in *Arabidopsis* development

Pamela A. Ribone, Matías Capella and Raquel L. Chan*

Instituto de Agrobiotecnología del Litoral, Universidad Nacional del Litoral, CONICET, CC 242 Ciudad Universitaria, 3000, Santa Fe, Argentina

* To whom correspondence should be addressed. E-mail: rchan@fbcb.unl.edu.ar

Received 27 January 2015; Revised 18 May 2015; Accepted 22 May 2015

Editor: Thomas Beeckman

Abstract

AtHB13 is a homeodomain leucine zipper I transcription factor whose function in development is largely unknown. *AtHB13* and *AtHB23* mutant and silenced lines were characterized by expression studies, reciprocal crosses, complementation, molecular analyses, and developmental phenotypes. The *athb13-1* and *athb13-2* mutants, *athb23* silenced, and *athb13/athb23* double-silenced plants exhibited faster elongation rates of their inflorescence stems, whereas only *athb13-1* and the double-knockdown *athb13/athb23* exhibited shorter siliques, fewer seeds, and unfertilized ovules compared with the wild type (WT). The cell sizes of mutant and WT plants were similar, indicating that these transcription factors probably affect cell division. Reciprocal crosses between *athb13-1* and the WT genotype indicated that the silique defect was male specific. Pollen hydration assays indicated that the pollen grains of the *athb13-1* mutant were unable to germinate on stigmas. *AtHB23*-silenced plants exhibited normal siliques, whereas double-knockdown *athb13/athb23* plants were similar to *athb13-1* plants. Both *AtHB13* and *AtHB23* were able to rescue the abnormal silique phenotype. *AtHB23* was upregulated in *athb13-2* plants, whereas its transcript levels in *athb13-1* mutants were not significantly increased. Transcriptome analysis comparing *athb13-1* and WT inflorescences revealed that a large number of genes, including several involved in pollen coat formation, are regulated by AtHB13. Finally, *athb13-1* complementation with mutated versions of *AtHB13* confirmed that two different tryptophans in its C terminus are essential. We conclude that AtHB13 and AtHB23 play independent, negative developmental roles in stem elongation, whereas only AtHB13 is crucial for pollen germination. Furthermore, AtHB23, which does not normally exert a functional role in pollen, can act as a substitute for AtHB13.

Key words: AHA motif, AtHB13, AtHB23, homeodomain leucine zipper, inflorescence stems, pollen hydration.

Introduction

Transcription factors (TFs) are proteins that are able to regulate entire signalling pathways. In plants, TFs are particularly abundant, representing approximately 6% of encoding genes (Ribichich *et al.*, 2014). This large group of proteins is divided into families and subfamilies according to their DNA-binding domains, in addition to other structural and functional features (Riechmann *et al.*, 2000; Mitsuda and Ohme-Takagi, 2009). In plants, proteins that contain homeodomains constitute a

Abbreviations: AHA, *a*romatic and large *h*ydrophobic residues embedded in an *a*cidic context; GUS, β-glururonidase; HD-Zip, homeodomain leucine zipper; miRNA, microRNA; qPCR, quantitative real-time PCR; RNA-Seq, RNA sequencing; RT, reverse transcription; TF, transcription factor; WT, wild type.

superfamily, which is divided into subfamilies depending on homeodomain sequence similarity and the presence of other conserved domains (Mukherjee *et al.*, 2009). Among these subfamilies, the homeodomain leucine zipper (HD-Zip) group is unique to plants and is divided into four subgroups, named I–IV (Ariel *et al.*, 2007). Members of group I are ~35 kDa proteins that present a conserved HD-Zip domain in the middle of their structures and have other putative functional motifs located at the C and N termini (Arce *et al.*, 2011). In several cases, the functionality of these motifs has been demonstrated experimentally (Lee *et al.*, 2001; Arce *et al.*, 2011; Zhang *et al.*, 2012; Sakuma *et al.*, 2013; Capella *et al.*, 2014).

With regard to their functions, HD-Zip I TFs have been associated primarily with abiotic stress and responses to changes in illumination conditions (Himmelbach *et al.*, 2002; Johannesson *et al.*, 2003; Wang *et al.*, 2003; Olsson *et al.*, 2004; Dezar *et al.*, 2005; Manavella *et al.*, 2006; Manavella *et al.*, 2008). In a few cases, they have been related to developmental and morphological events. In this sense, LMI1, an *Arabidopsis* HD-Zip I TF, acts in regulating meristem identity by targeting LFY, affecting leaf shape and bract formation (Saddic *et al.*, 2006). The HD-Zip I TF VRS1 is responsible for a six-rowed phenotype in barley plants bearing the recessive allele *vrs1* (Komatsuda *et al.*, 2007), whereas a mutation in the pea *TL* gene generates plants with a particular phenotype: leaflets take the place of tendrils (Hofer *et al.*, 2009). However, in the majority of studies, HD-Zip I proteins have been related to response mechanisms to environmental conditions and not to developmental events.

In *Arabidopsis thaliana*, AtHB13 and its paralogue AtHB23 were classified as group V in a recent HD-Zip I phylogenetic reconstruction (Arce *et al.*, 2011). These TFs exhibit 78% sequence identity in their HD-Zip domains and their expression patterns are very similar; both have been detected in the shoot meristem region, leaf junction, basal parts of petals, sepals and stamens, and within the stigma (Hanson *et al.*, 2002; Kim *et al.*, 2007). However, they are differentially regulated: *AtHB13* is upregulated in response to drought, salinity stress, and low temperatures (Cabello and Chan, 2012; Cabello *et al.*, 2012), whereas *AtHB23* is downregulated by abscisic acid and NaCl treatments (Henriksson *et al.*, 2005), indicating that these paralogues are probably playing different roles. Plants that overexpress *AtHB13* have been shown to be involved in the regulation of cotyledon and leaf development in response to carbon availability during early developmental stages (Hanson *et al.*, 2001). In recent studies, it was demonstrated that plants overexpressing *AtHB13* were able to tolerate freezing temperatures, severe drought, and salinity stresses through cell membrane stabilization (Cabello and Chan, 2012; Cabello *et al.*, 2012). Plants overexpressing this HD-Zip I TF are also resistant to infections with downy mildew (*Hyaloperonospora arabidopsidis*) and green peach aphids (*Myzus persicae*; Gao *et al.*, 2014). On the other hand, AtHB23 has been reported as a phytochrome B-interacting protein, and *athb23* mutant plants exhibit long hypocotyls, defects in seed germination, and cotyledon expansion under red light; therefore, *AtHB23* has been suggested to be involved in red-light sensing mediated by phyB (Choi *et al.*, 2014).

Although these studies have contributed to our understanding of the functions of AtHB13 and AtHB23, the roles of these proteins in different developmental stages and the extent of the relationship between these paralogous genes remain largely unknown. A recent study that was conducted by our group demonstrated that another paralogous HD-Zip I pair, AtHB7 and AtHB12, finely regulate each other during development and after stress treatments (Ré *et al.*, 2014). To determine whether this was also true in the case of AtHB13 and AtHB23, and aiming to understand the role of these genes in *Arabidopsis*, simple mutants and double-knockdown plants were created and thoroughly analysed. Surprisingly, a crucial role in development that was unrelated to environmental conditions was assigned to AtHB13. Analysis of the obtained experimental data led us to propose a model in which AtHB13 plays a key role in a plant reproductive stage, more precisely in pollen germination, whereas both paralogues have roles in inflorescence stem elongation. Regarding pollen germination, when AtHB13 is severely downregulated, AtHB23 is able to replace it and can rescue a wild-type (WT) phenotype, even though it normally does not have a role in this process.

Materials and methods

Plant material and growth conditions

A. thaliana ecotype Columbia (Col-0) (WT) plants were grown directly in soil in a growth chamber at 22–24 °C under a long-day photoperiod (16 h light) at an intensity of approximately 120 µmol m^{-2} s^{-1} in 8 × 7 cm pots for 40 d. Mutant seeds with the T-DNA insertions *athb13-1* (SAIL_893_G05) and *athb13-2* (GABI_859H06) on a Col-0 ecotype background were obtained from the *Arabidopsis* Biological Resource Center (http://www.arabidopsis.org) and NASC (http://arabidopsis.info/), respectively. Homozygous lines were selected after two complete growth cycles.

Genetic constructs

35S::AtHB13 AtHB13 cDNA was cloned into *pDONR221* as described by Cabello *et al.* (2012) and then cloned into a pK2GW7 vector via GATEWAY recombination with LR Gateway® Clonase II enzyme mix (Invitrogen).

35S::AtH23 Constructs were obtained after amplification of cDNAs with specific oligonucleotides using a U23330 clone as template, which was obtained from the *Arabidopsis* Biological Resource Center (Supplementary Table S3, available at *JXB* online). The amplification product was cloned into *Bam*HI and *Xho*I sites in a pENTR3C plasmid and was finally cloned into the pK2GW7 vector by GATEWAY recombination as above.

35S::amiR13/23 *and* 35S::amiR23 Artificial microRNAs (miRNAs) were designed as described by Schwab *et al.* (2006) (http://wmd3.weigelworld.org/cgi-bin/webapp.cgi). A PCR pRS300 vector was used as a template, and specific oligonucleotides were designed (Supplementary Table S3). The resultant fragments were cloned into *Sal*I and *Xba*I sites in the pENTR3C plasmid and then cloned into the pK2GW7 plasmid by GATEWAY recombination as above. Double *AtHB13*/*AtHB23* silenced plants were named *amiRNA13/23*, and plants silenced for *AtHB23* were named *amiRNA23*.

At13ΔC, At13ΔAHA, At13WxA, *and* At13D289A These constructs were created by subcloning portions of *AtHB13* cDNA into *Xba*I and *Bam*HI sites of a pBI122 plasmid as described by Capella

et al. (2014). These DNA segments were amplified previously with the oligonucleotides that are described in Supplementary Table S3.

pAtHB13::GUS A fragment that lies 1772 bp upstream of the start codon of *AtHB13* was amplified from WT genomic DNA using specific oligonucleotides (Supplementary Table S3). The amplification product was cloned into a pGEM-T Easy vector and then subcloned into *Sal*I and *Xba*I sites in a pENTR3C plasmid. Finally, the promoter region was cloned into a pKGWFS7 vector by GATEWAY recombination as above.

Stable transformation of Arabidopsis *plants*

A transformed *Agrobacterium tumefaciens* strain, LBA4404, was used to create transgenic *Arabidopsis* plants via a floral dip procedure (Clough and Bent, 1998). Transformed plants were selected on the basis of their resistance in Petri dishes with 0.5× Murashige and Skoog medium supplemented with vitamins (PhytoTechnology Laboratories) and the appropriate selector chemicals (50 mg l^{-1} of Basta, 50 mg l^{-1} of kanamycin, or 7.5 mg l^{-1} of sulfadiazine). The seeds were surface sterilized, plated, and placed in a growth chamber at 22–24 °C after 2 d of incubation at 4 °C.

Transgene insertions were verified by PCR using genomic DNA as a template and specific oligonucleotides for each of the constructs described above. Three or four positive independent lines were further reproduced, and homozygous T3 and T4 plants were used to analyse transgene expression levels and plant phenotypes.

RNA extraction and analysis

Total RNA for use in reverse transcription quantitative real-time PCR (RT-qPCR) was isolated from *Arabidopsis* inflorescences using Trizol® reagent (Invitrogen) according to the manufacturer's instructions. One microgram of RNA was reverse transcribed using oligo$(dT)_{18}$ and Moloney murine leukemia virus reverse transcriptase II (Promega). qPCR was performed using a Mx3000P Multiplex qPCR system (Stratagene, La Jolla, CA, USA); each reaction contained a 20 µl final volume that included 2 µl of SyBr Green (4×), 8 pmol of each primer, 2 mM $MgCl_2$, 10 µl of a 1/15 dilution of the reverse transcription reaction and 0.1 µl of *Taq* Platinum (Invitrogen). Fluorescence was measured at 72 °C over 40 cycles. Specific primers were designed (Supplementary Table S3). Quantification of mRNA levels was achieved by normalization against actin transcript levels (*ACTIN2* and *ACTIN8*) according to the $\Delta\Delta C_t$ method. All of the reactions were performed with at least three replicates.

Inflorescence stem length assays

Inflorescence stem lengths were measured using a ruler over a course of 14 d; time 0 represented the first day of bolting. Plant materials for histological cuts were fixed in 50% (v/v) ethanol, 5% (v/v) acetic acid, and 3.7% v/v formaldehyde for 16 h and then dehydrated with ethanol and embedded in Histoplast (Biopack). Sections (10 µm thick) were mounted on slides coated with 50 µg ml^{-1} of poly-D-lysine (Sigma Chemical Co., St Louis, MO, USA) in 10 mM Tris/HCl, pH 8.0, and dried overnight at 37 °C. The paraffin was removed with xylene, and the sections were rehydrated. Staining was performed with methylene blue. Images were taken using a Nikon Coolpix L810 camera under microscopy (Nikon Eclipse E200).

Histochemical β*-glucuronidase (GUS) staining*

GUS staining was performed as described by Jefferson *et al.* (1987). Plants were immersed in GUS staining buffer (1 mM 5-bromo-4-chloro-3-indolyl-glucuronic acid in 100 mM sodium phosphate, pH 7.0, 0.1% Triton X-100, 100 mM potassium ferrocyanide, 100 mM potassium ferricyanide), a vacuum was applied for 5 min, and plants were then incubated at 37 °C for 12 h. Chlorophyll was cleared from the plant tissues by immersion in 70% ethanol.

Silique phenotype analyses

Siliques were detached and photographed, and their lengths were quantified using ImageJ software (http://rsbweb.nih.gov/ij/). To quantify unfertilized ovules, the siliques were dissected under a Nikon SMZ800 stereomicroscope, and the numbers of fertilized and unfertilized ovules were counted.

Pollen assays

Pollen tube emergence was assayed in 1 ml of pollen germination medium according to Boavida and McCormick (2007). Pollen from a mature anther was poured and dusted onto a microscope slide and then incubated in a moisture chamber. Hydration assays were performed on emasculated flower buds, which were hand pollinated under a Nikon SMZ800 stereomicroscope according to Mayfield and Preuss (2000). Pollen width was measured upon contact with the stigma and throughout hydration by taking pictures every 15 s under microscopy.

For pollen tube staining with aniline blue, pistils were detached 24 h after pollination and then fixed for 1 h in ethanol:acetic acid (3:1), washed with water, softened with 4 M NaOH for 1 h, cleared with 50% NaClO, and then stained with 0.1% decolorized aniline blue (in 0.1 M K_2HPO_4 buffer) for 4 h. Finally, pistils were washed briefly with water and mounted onto a microscope slide using a mix of 0.1% aniline blue and 50% glycerol. Aniline blue fluorescence was visualized under a Nikon Eclipse E200 microscope equipped with a Nikon Coolpix L810 camera.

RNA sequencing (RNA-Seq)

RNA for RNA-Seq was isolated via TRI Reagent extraction with clean-up using columns from a Qiagen Plant RNeasy Mini kit. A total of 10 µg of each sample was sent to the Genome Technology Access Center at the Washington University School of Medicine where mRNA was extracted from total RNA using a Dynal mRNA Direct kit (Life Technology). mRNAs were then fragmented and reverse transcribed into double-stranded cDNA using random primers before the addition of adapters. Sequencing was performed using HiSeq 2500 equipment. The resultant fastQ files were then aligned with the most recent *Arabidopsis* Col-0 genome assembly (TAIR10; released in June 2009) with TopHat version 2.0.8 using Bowtie2 version 2.1.0.

Confocal microscopy

Images were obtained using a Leica TCS SP8 confocal laser microscope. Samples were excited using a 488 nm laser, and emission was detected in two channels: 510–530 nm for green fluorescent protein (GFP) and 540–600 nm for lignin autofluorescence. To eliminate lignin autofluorescence leaking into GFP analyses, images were processed using ImageJ v.1.47 software.

Results

athb13 *mutant plants exhibit a differential developmental phenotype in the reproductive stage*

With the aim of unravelling the function of *AtHB13*, two homozygous *athb13* mutants were created. The first line, *athb13-1*, possessed a T-DNA insertion at its 3′ untranslated region, whereas the second line, *athb13-2*, possessed a T-DNA insertion inside its leucine zipper-coding region (Fig. 1A). The *AtHB13* transcript levels in these mutants were measured by RT-qPCR using oligonucleotides that matched the homeodomain region; transcript levels were lower than in WT plants but were still detectable. The first mutant exhibited

a 40% reduction in *AtHB13* transcript levels, whereas the second mutant exhibited a 90% reduction in *AtHB13* transcript levels compared with the WT genotype (Fig. 1B).

Neither of the two mutants exhibited any alterations in morphological or developmental phenotypes compared with WT during the vegetative stage when grown in standard conditions (Fig. 2A). However, after bolting, both mutant lines exhibited faster stem elongation and, ending the life cycle, longer inflorescence stems (Fig. 2B), indicating that AtHB13 has a negative role in stem elongation. Moreover, *athb13-1* plants exhibited obviously shorter siliques (Fig. 2C). Notably, neither anthers nor carpels showed any developmental defects compared with WT plants. Unexpectedly, siliques from *athb13-2* mutants were not significantly different than those of control plants (Fig. 2C). This observation was puzzling because *AtHB13* transcript levels were 10% of those of WT plants and were clearly lower in the *athb13-2* versus *athb13-1* mutants.

To understand better the observed differential phenotypes, the expression patterns of *AtHB13* were surveyed in transgenic plants in which the *AtHB13* promoter (a 1700 bp fragment upstream of the start codon) controlled the reporter genes *GFP* and *GUS*. GUS expression was evident in the base of the inflorescence stem at the bolting moment and during the following days. In mature plants, GUS was expressed in the upper portions of inflorescence stems (Fig. 3A). Conversely, GFP fluorescence was clearly visualized in the anthers of flowers at stage 12 and later decreased (Fig. 3B). These observations were consistent with the phenotype described above, indicating that *AtHB13* has a role in development.

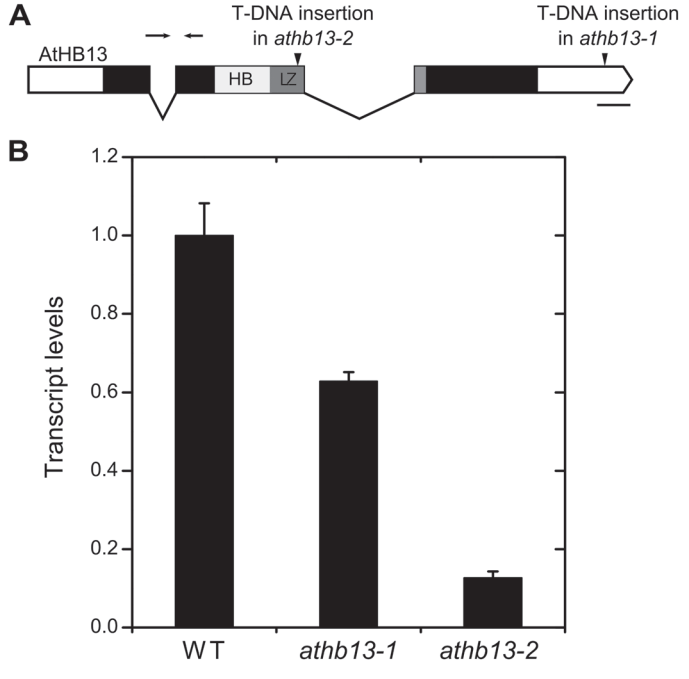

Fig. 1. *AtHB13* is downregulated to different extents in two different mutants. (A) Schematic representation of the *AtHB13* gene. White boxes represent 5′ and 3′ untranslated regions; filled boxes represent exons; lines represent introns. Arrowheads indicate the locations of T-DNA insertions in each mutant. Arrows indicate the binding sites of the primers used in RT-qPCR. HB, homeobox; LZ, leucine zipper. Bar, 100 bp. (B) Relative transcript levels of *AtHB13* in 40-d-old inflorescences. Total RNA was isolated from inflorescences and analysed by RT-qPCR with specific oligonucleotides (Table S3). Transcript levels were normalized by applying the $\Delta\Delta C_t$ method. Error bars represent standard error calculated from three independent biological replicates. Actin transcripts (*ACTIN2* and *ACTIN8*) were used as references.

Inflorescence stems elongate faster in athb13 *mutant plants*

To characterize further the observed differential phenotype, kinetic analysis of inflorescence stem elongation was performed (Fig. 4A). In both of the mutant genotypes (*athb13-1* and *athhb13-2*), stems elongated faster starting in the bolting

Fig. 2. *athb13* mutant plants exhibit longer inflorescence stems and shorter siliques compared with WT plants. (A) Illustrative photographs of 17-d-old WT, *athb13-1*, and *athb13-2* plants. (B) Photographs of 35-d-old WT, *athb13-1*, and *athb13-2* plants. (C) Siliques of WT, *athb13-1*, and *athb13-2* plants at stage 17b (Roeder and Yanofsky, 2006).

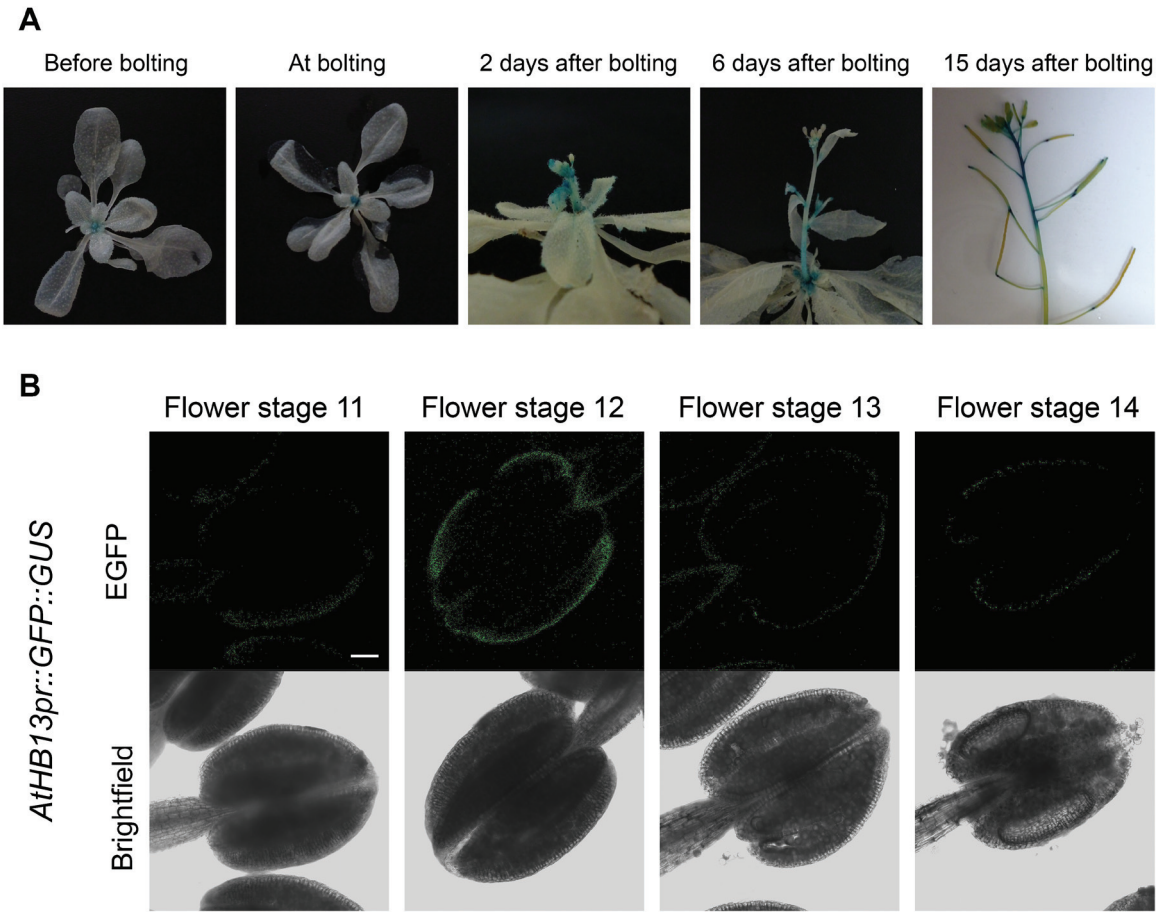

Fig. 3. Expression kinetics of *AtHB13* after bolting. (A) Histochemical detection of GUS enzymatic activity in *pAtHB13::GFP::GUS* plants at the indicated developmental stages; pAtHB13 included a 1700 bp DNA fragment upstream of the translation start codon. (B) GFP visualization in *pAtHB13::GFP::GUS* anthers at different developmental stages. Images were obtained with a confocal laser microscope. Bar, 40 μm.

moment compared with WT. This growth rate difference was maintained during the following 14 d and until plants reached a mature stage, which resulted in longer stems in the mutant genotypes (Figs 2B and 4A and Supplementary Fig. S1, available at *JXB* online). The differences in length were particularly evident in the stem segment that was limited by the upper node and the flower, and were very similar in the segment between the rosette and the upper node (Fig. 4A).

The differential phenotypes that were observed in *athb13-1* and *athb13-2* could be a consequence of a secondary T-DNA insertion; in such a case, the observed phenotype would be independent of *AtHB13*. To explore this possibility, we transformed *athb13-1* homozygous plants with a construct bearing the *AtHB13* coding region under the control of a 35S cauliflower mosaic virus promoter (*35S::AtHB13*). Two independent transgenic lines were evaluated and were indistinguishable from WT regarding inflorescence stem elongation (Fig. 4B and Supplementary Fig. S1), which strongly indicated that the observed phenotype was indeed a consequence of the *AtHB13* mutation.

AtHB23, a paralogue of AtHB13, also negatively regulates inflorescence stem growth

Regarding the inflorescence stem differential phenotype that was exhibited by both of the *athb13* mutants and the ability of *AtHB13* to rescue it, we sought to determine whether *AtHB23*, a paralogue gene of *AtHB13*, was also involved in this developmental process. AtHB23 shares 62% identity with AtHB13 and possesses a similar expression pattern (Arce *et al.*, 2011); however, no suitable *athb23* mutant plants were available in public resources, and the only one available had an additional insertion in *AtATH3*. Considering the time-consuming and difficult process that would be required to isolate an *athb23* mutant out of this double mutant, we decided instead to create silenced plants using artificial miRNAs. Therefore, an artificial miRNA was constructed to achieve knockdown of *AtHB23* in a WT background, and an additional miRNA was designed to obtain a double *athb13*/*athb23* knockdown genotype (Supplementary Fig. S2A, available at *JXB* online). Expression levels of *AtHB23* were clearly repressed in both the single and double-knockdown transgenic plants, whereas the expression levels of AtHB13 changed only in the double mutant (Supplementary Fig. S2B). The inflorescence stems of these plants were examined (Fig. 4C), as well as their elongation kinetics after bolting (Fig. 4D). All three of the silenced genotypes possessed more elongated inflorescence stems than WT plants, and their growth kinetics were similar to those exhibited by both of the *athb13* mutants (Fig. 4A). These observations indicated that both paralogues are independently involved in this developmental process and exert negative roles.

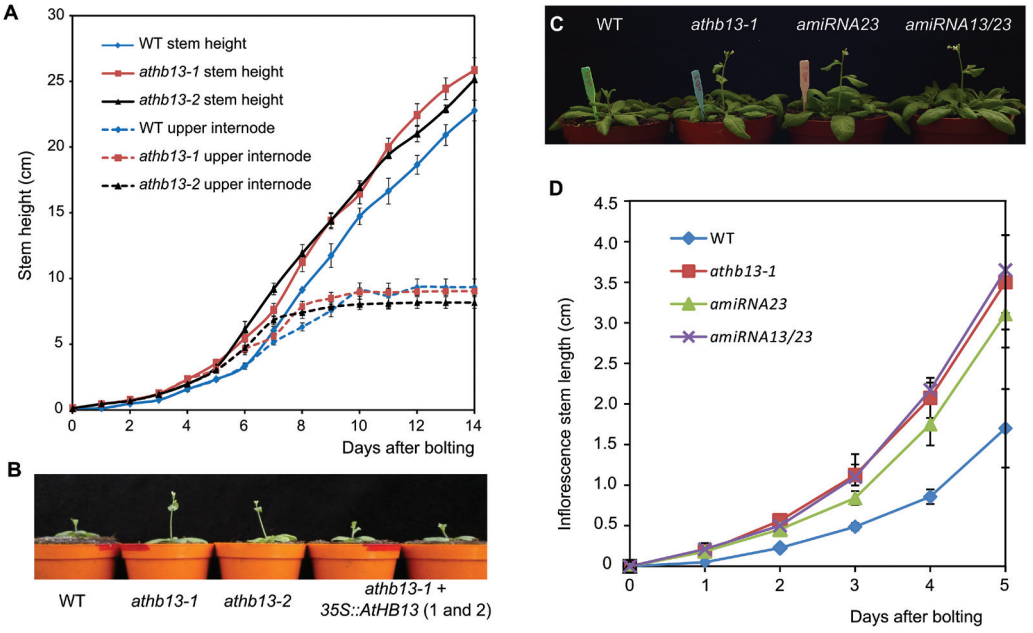

Fig. 4. AtHB13 and AtHB23 play negative roles in inflorescence stem growth. (A) Kinetics of stem elongation in WT, *athb13-1*, and *athb13-2* plants. Time 0 represents the day on which bolting was visualized. Stems and internodes were measured with a ruler. Each point represents the mean inflorescence stem length of 16 plants. Bars represent standard error. (B) Representative images taken 4 d after bolting in WT, *athb13-1*, *athb13-2*, and two independent lines of *athb13-1* that were transformed with *35S::AtHB13*. (C) Illustrative photographs of 25-d-old WT, *athb13-1*, *amiRNA23*, and *amiRNA13/23* plants showing differences in inflorescence stem lengths. (D) Kinetics of inflorescence stem elongation in the different genotypes after bolting. Time 0 represented the bolting day. Each point represents the mean inflorescence stem length of 16 plants. Bars represent standard error.

The inflorescence stem phenotype of athb13 *mutants is probaby due to differential cell division*

To determine whether the above differences were due to a higher rate of cell division or to variations in cell sizes, histological sections were obtained from different regions of the stems (Fig. 5A). Cell length was measured under microscopy, but no significant differences between genotypes were detected, indicating that the rate of cell division was probably increased in *athb13* mutants (data not shown).

To further assess this differential phenotype, the expression of five different cyclin-encoding genes and five genes encoding proteins involved in cell expansion was evaluated in *athb13-1* mutant and WT plants. The cyclin-encoding genes were upregulated in the mutant genotype (Fig. 5B), whereas the transcripts of *PMEI* (*PLANT INVERTASE/PECTIN METHYLESTERASE INHIBITOR SUPERFAMILY PROTEIN*,), *CESA10* (*CELLULOSE SYNTHASE 10*), *EXP10* (*EXPANSIN 10*), and *XTH15* (*XYLOGLUCAN ENDOTRANSGLUCOSYLASE/HYDROLASE 15*) did not show significant differences between *athb13-1* and WT plants (Fig. 5C). Only *PLP4* (*PATATIN-LIKE PROTEIN 4*; Li *et al.*, 2011), known as a cell expansion repressor, was upregulated in the mutant. These observations supported a negative role of AtHB13 in the inflorescence stem elongation by repressing cell division (Fig. 5B).

athb13-1 *mutant plants exhibit abnormal ovule fertilization*

In addition to the differences in inflorescence stem elongation rates described above, another interesting differential phenotype was visualized in *athb13-1* plants: they exhibited shorter siliques (Fig. 2C). Deeper analysis of these siliques revealed that they had fewer viable embryos, which were localized primarily in the upper portion of the fruit, although the total number of ovules was equal between mutant and WT genotypes (Fig. 6A, B). Notably, *athb13-2* mutant plants were indistinguishable from WT regarding silique sizes and quantities of ovules.

An important question that arose following the visualization of the decreased number of embryos in *athb13-1* mutants was whether this defect was male or female specific. To answer this question, we performed reciprocal crosses between WT and *athb13-1* plants. When WT stigmas were pollinated with *athb13-1* pollen, the mutant phenotype was still observed. In contrast, when *athb13-1* stigmas were pollinated with WT pollen, normal seed development occurred, indicating that the defective phenotype was clearly male specific and caused by the pollen donor (Fig. 6C). Aniline blue staining of carpels 24 h after pollination confirmed that only a few grains of *athb13-1* pollen were able to germinate on both mutant and WT stigma surfaces. Moreover, pollen tubes only reached the upper part of the ovary (Supplementary Fig. S3A, available at *JXB* online). Consistently, less than 10% of *athb13-1* pollen grains were able to germinate and form fully elongated pollen tubes *in vitro* (Supplementary Fig. S3B).

Pollen of athb13-1 *mutants exhibits an abnormal interaction with the stigma*

Three major events occur in *Arabidopsis* prior to pollen germination and after a pollen grain lands on the stigma: pollen

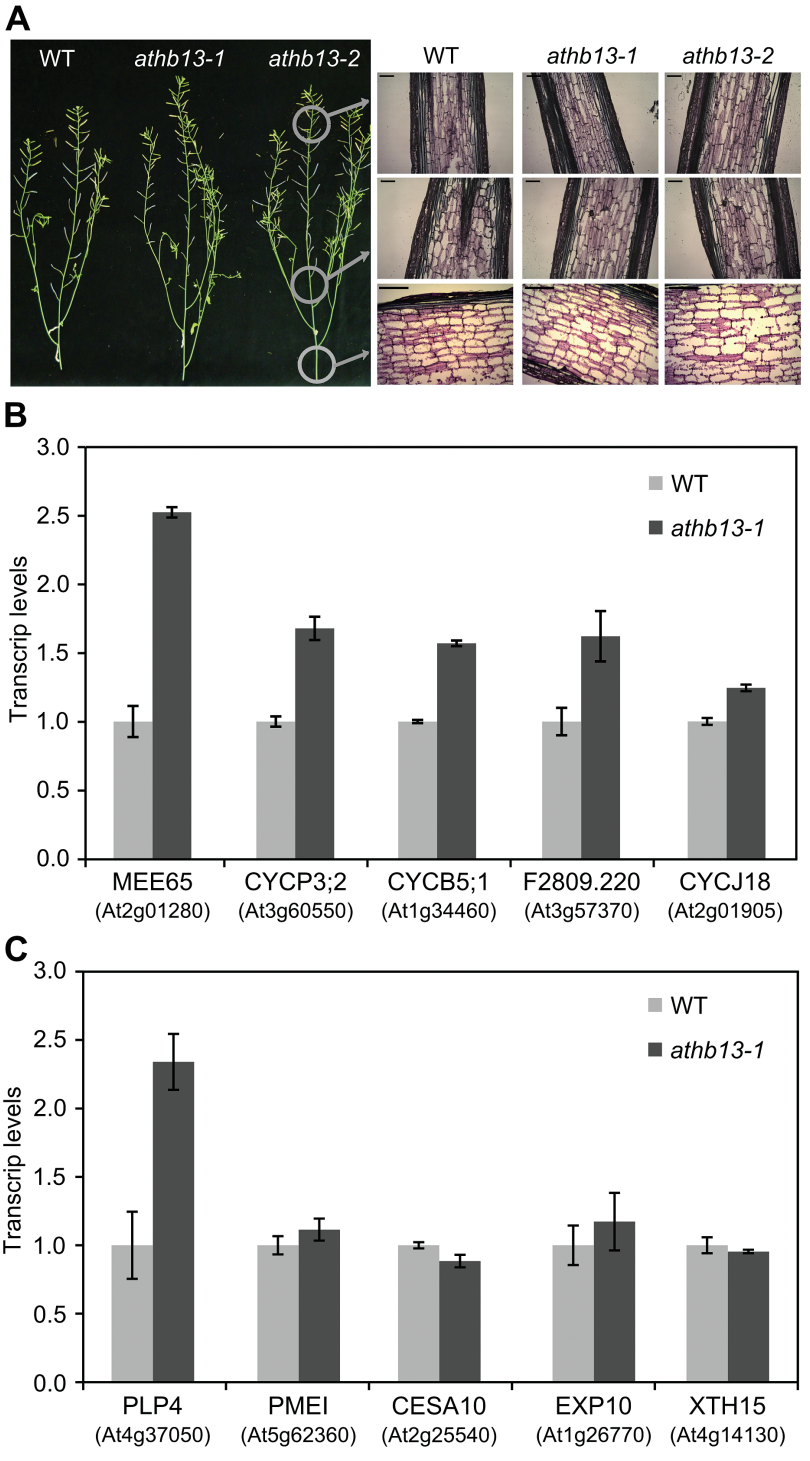

Fig. 5. Cell division is probably responsible for the differences in stems length exhibited by *athb13-1* mutant plants. (A) Left panel: illustrative photographs of 35-d-old WT, *athb13-1*, and *athb13-2* plants in which the sections that were taken for histological analyses are indicated with circles. Right panel: histological sections of inflorescence stems stained with methylene blue. Bars, 0.25 mm. (B, C) Differential expression in WT and *athb13-1* mutant plants of five genes encoding cyclins involved in cell division (B) and five genes involved in cell expansion (C). Transcript levels were normalized by applying the $\Delta\Delta C_t$ method. Error bars represent standard deviation calculated from three independent biological replicates. Actin transcripts (*ACTIN2* and *ACTIN8*) were used as references.

adhesion, foot formation, and pollen hydration. Knowing that a group of genes that are involved in pollen hydration was differentially regulated in *HaHB1* (a sunflower orthologue of *AtHB13*) overexpressor plants (Cabello *et al.*, 2012), we decided to evaluate pollen hydration ability. Hydration was tested directly on stigmas, allowing us to observe that both WT and *athb13-1* pollens initiated hydration at the same time; however, WT pollen grains reached significantly larger sizes than those of *athb13-1* (Fig. 7). Regarding these results, it could be concluded that *athb13-1* pollen failed to interact with the stigma, even in the case of WT stigma (not shown). Moreover, unlike other mutants that have been described as

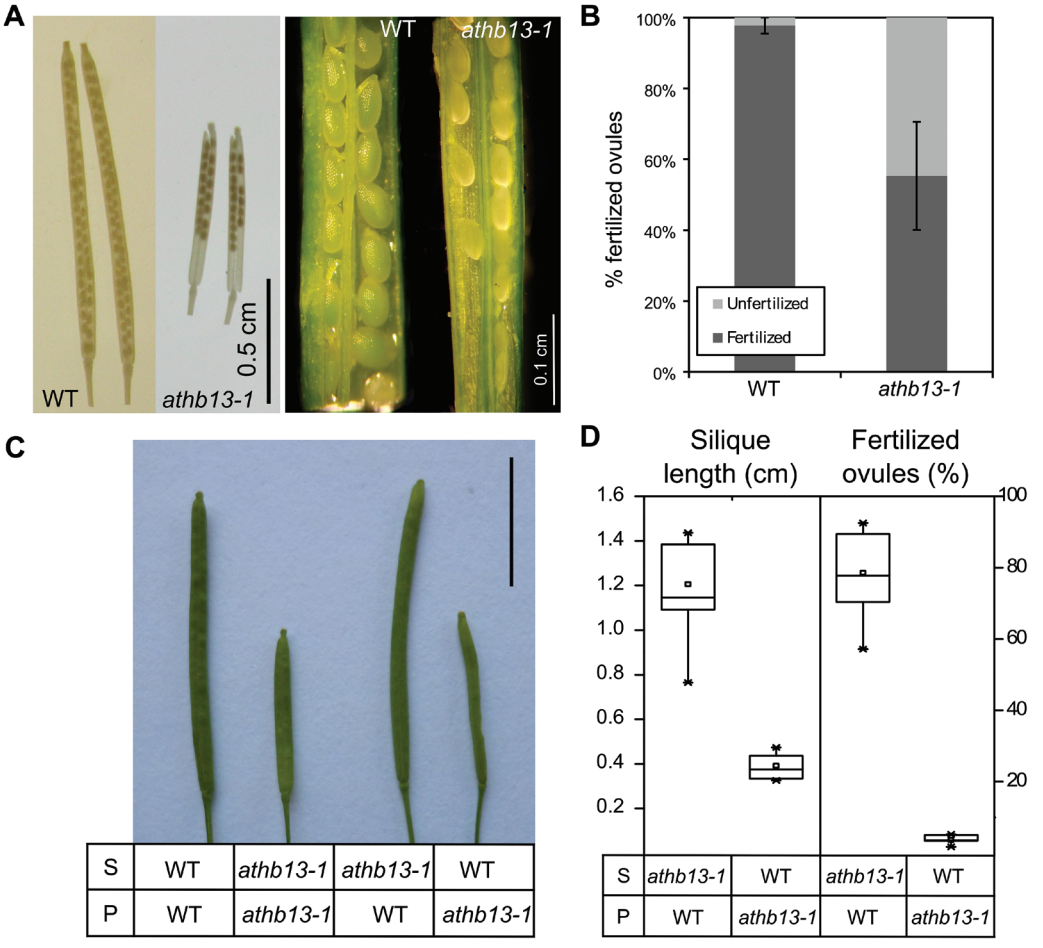

Fig. 6. *athb13-1* mutant plants exhibit unfertilized ovules and shorter siliques due to a pollen defect. (A) Left panel: unstained siliques of WT and *athb13-1* plants at stage 18 (Roeder and Yanofsky, 2006). Right panel: illustrative photograph of the inside of the siliques. (B) Quantitation of fertilized and unfertilized ovules. The experiment was conducted using 15 siliques per genotype ($P<0.001$). Bars represent standard deviation. (C) Illustrative photograph of siliques obtained from the cross-pollination of WT and *athb13-1*, changing the donors of stigma and pollen as indicated at the bottom; flowers were at stage 12 (Smyth *et al.*, 1990) and $n=15$. S, stigma; P, pollen. Bar, 0.5 cm. (D) Box plot showing silique lengths and percentage of fertilized ovules per silique obtained from the same cross-pollinations as indicated at the bottom ($n=15$ per cross; $P<0.001$).

being defective in pollen hydration (Mayfield and Preuss, 2000; Updegraff *et al.*, 2009), *athb13*-1 plants did not show a delay in hydration; the major difference compared with WT was the amount of absorbed water, which was evaluated by the fold change in pollen grain diameter versus that measured at time 0 (Fig. 7B). Conversely, although pollen adhesion was tested in mutant and WT plants, no differences between genotypes were detected in this process (Supplementary Fig. S3).

The fact that only *athb13-1* and not *athb13-2* exhibited the silique phenotype was disconcerting. Although the differential stem elongation was complemented with AtHB13, this pollen defect could still be a consequence of a secondary T-DNA insertion. To explore this possibility, we analysed *athb13-1* homozygous plants that were complemented with *35S::AtHB13* constructs. Four out of five of the transgenic lines of the F1 progeny no longer showed the hydration defect and exhibited hydration curves similar to those of WT pollen (Fig. 7B), indicating that the observed phenotype was indeed a consequence of the *AtHB13* mutation.

Considering these results, it was still disconcerting that *athb13-2* mutants did not show any particular phenotype regarding silique development, as discussed above. Moreover, when these mutant plants were tested for pollen germination by aniline blue staining, the pollen grains normally germinated on the stigma and pollen tubes reached the bottom of the carpel (Supplementary Fig. S4, available at *JXB* online). However, a difference with WT pollen was detected: approximately 50% of the pollen grains exhibited a clear delay until they were hydrated (Supplementary Fig. S5, available at *JXB* online).

Transcriptomic analysis of WT and athb13-1 *inflorescences reveals differentially expressed genes involved in cell wall differentiation and transport*

With the aim unravelling the molecular mechanisms involved in the abnormal pollen germination phenotype that was observed in the *athb13-1* mutants, an RNA-Seq transcriptomic analysis was performed using RNA extracted from WT and *athb13-1* inflorescences. Instead of isolated pollen, whole inflorescences were used as the material for this study because it has been described previously that several of the genes that are involved in the pollen hydration process are not expressed in pollen itself but are instead expressed in the

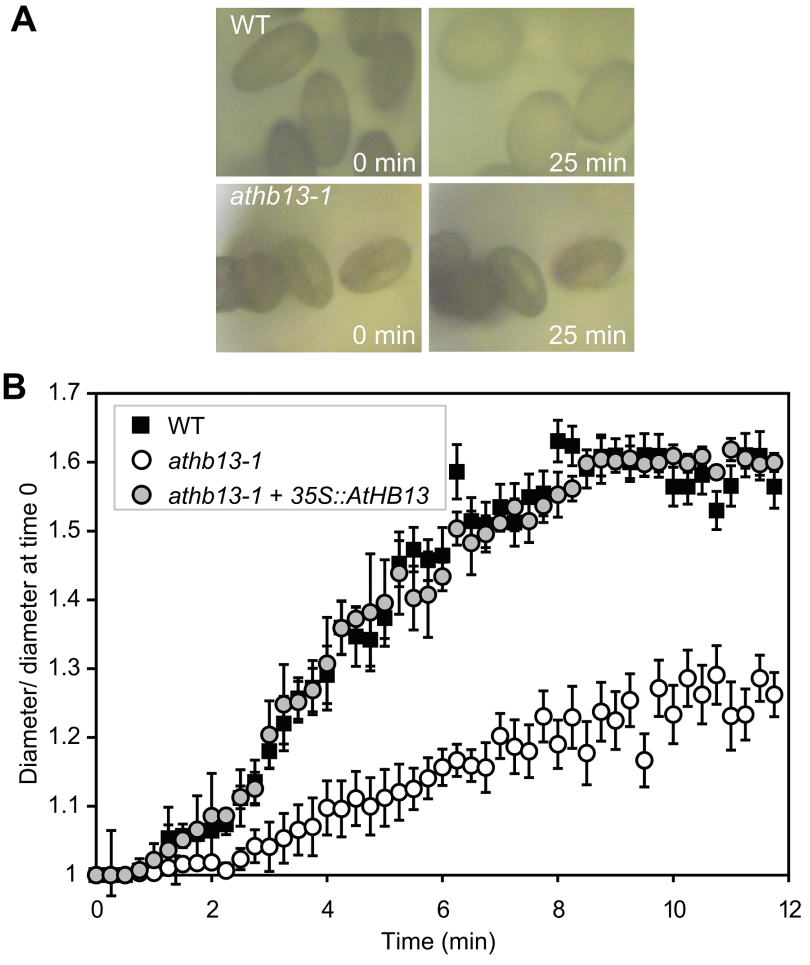

Fig. 7. *athb13-1* mutant pollen hydration is defective. (A) Pictures showing hydration of WT and *athb13-1* pollen grains on the stigma. (B) Time course of pollen hydration on the stigmas of WT, *athb13-1*, and *athb13-1* plants transformed with *35S::AtHB13*. Flowers were tested at stage 12 (Smyth *et al.*, 1990). Images were captured every 15 s. Each point represents *n*=10 pollen grains. Bars represent standard deviation.

tapetum (Mayfield and Preuss, 2000; Mayfield *et al.*, 2001; Updegraff *et al.*, 2009; Loraine *et al.*, 2013).

As expected, *AtHB13* transcript levels were lower in mutant versus WT inflorescences. Notably, the coverage of *AtHB13* transcripts was very similar in both genotypes until the T-DNA insertion was reached, indicating that the coding sequence in the mutant was complete (Supplementary Fig. S6, available at *JXB* online). A total of 800 different genes were detected as being differentially expressed, and 323 of them exhibited at least a 2-fold change (Supplementary Table S1, available at *JXB* online). Unfortunately, the majority of these genes were classified as being of unknown function (Supplementary Fig. S7, available at *JXB* online). Notably, a considerable number of genes that were described as pollen coat genes (Mayfield *et al.*, 2001) belonged to the GRP family and were found to be slightly repressed in the mutant, in addition to EXL3. Even when the repression was only approximately 30%, the fact that all of these genes exhibited the same behaviour could be significant. The others were identified as genes that are involved in cell development and organization; several of them are related to pollen germination, pollen tube cell wall modification, and directional growth, and represent the strongest candidates for causing the observed phenotype (Supplementary Table S2, available at *JXB* online). Another of the groups of regulated genes encoded transport proteins, and it is well known that pollen germination on the stigma is mediated by the transport of several proteins and lipids (Bock *et al.*, 2006; Komarova *et al.*, 2008). A curious observation regarding the subcellular localization of the encoded proteins was that most of the known proteins localized to extracellular space, consistent with pollen–stigma communication (Supplementary Fig. S7). Interestingly, only 36 out of the 312 differentially expressed genes were induced, indicating that AtHB13 is probably acting as an activator of gene expression. On the other hand, 28 of the differentially expressed genes possessed in their promoter regions the pseudo-palindromic sequence CAATNATTG, which is recognized by HD-Zip I TFs. Validation of the RNA-Seq assay was achieved by RT-qPCR, and the results indicated a positive correlation (Supplementary Fig. S7).

AtHB23 is able to replace AtHB13 function in flower development

Considering the clear and disconcerting phenotypic differences that were observed between *athb13-1* and *athb13-2* mutants and that a second T-DNA insertion was not the mechanism responsible for them, we proposed two different

hypotheses. Knowing that a pair of HD-Zip I TFs, AtHB7 and AtHB12, regulate each other to fine-tune processes that are associated with growth and stress responses (Ré *et al.*, 2014), the first hypothesis was that in *athb13-1* mutant plants the levels of *AtHB13* transcripts are sensed as being sufficient, even if they are not,whereas in *athb13-2* mutant plants, the levels of *AtHB13* transcripts are sensed as being insufficient and therefore the paralogue *AtHB23* is upregulated to replace the function of AtHB13. The second hypothesis was that a neomorphic AtHB13 protein was translated and that this protein was unable to function; however, because it occupies the target sites of AtHB13, the putative redundant AtHB23 would not be able to replace it, resulting in the abnormal phenotype.

The first step in investigating which of these hypotheses could be corroborated was to measure *AtHB23* transcript levels in inflorescences of *athb13-1* and *athb13-2* mutants. The results indicated that, even in *athb13-1* plants, *AtHB23* was slightly upregulated; transcript levels of this gene in *athb13-2* plants were significantly higher (Fig. 8A), supporting the first hypothesis stated above.

Secondly, pollen hydration tests were performed with the silenced *athb23* and *athb13/athb23* genotypes and indicated that a lack of *AtHB23* only was not sufficient to generate abnormalities in pollen hydration (Fig. 8B). Nevertheless, when both *AtHB13* and *AtHB23* were silenced, the resulting pollen hydration phenotype was defective in a manner that was similar to the simple *athb13-1* mutant (Fig. 8B).

Further and more robust evidence about the role that *AtHB23* has in replacing *AtHB13* was obtained from experiments in which *athb13-2* plants, which were not exhibiting a defective pollen phenotype, were transformed with miRNA against *AtHB23*. These plants produced the same level of defectiveness as *athb13-1* plants, indicating that when both paralogues are downregulated, pollen was unable to hydrate in contact with the stigma (Fig. 8C). Similarly, *35S::AtHB23* was able to rescue the abnormal phenotypes of *athb13-1* plants (Fig. 8C).

Two tryptophans of the AHA motif of AtHB13 are essential for it to exert its function

HD-Zip I TFs exhibit an AHA (*a*romatic and large *h*ydrophobic residues embedded in an *a*cidic context)-like transactivation motif in their C termini (Arce *et al.*, 2011). The AHA motif of AtHB13 and, in particular, the tryptophans present in this motif have been demonstrated as essential for transcriptional activation in yeast and *Arabidopsis* (Capella *et al.*, 2014). However, no functionality related to a certain phenotype has been indicated thus far. Considering the abnormal reproductive phenotypes presented by *athb13-1* and *athb13-2* mutant plants and that these abnormalities were completely rescued by transformation with a *35S::AtHB13* construct, we decided to test the ability of different constructs, which had deletions or mutations in the AHA motif, to rescue the defect. Transformed plants were created, and their stems and inflorescences were evaluated (Fig. 9). Constructs in which the

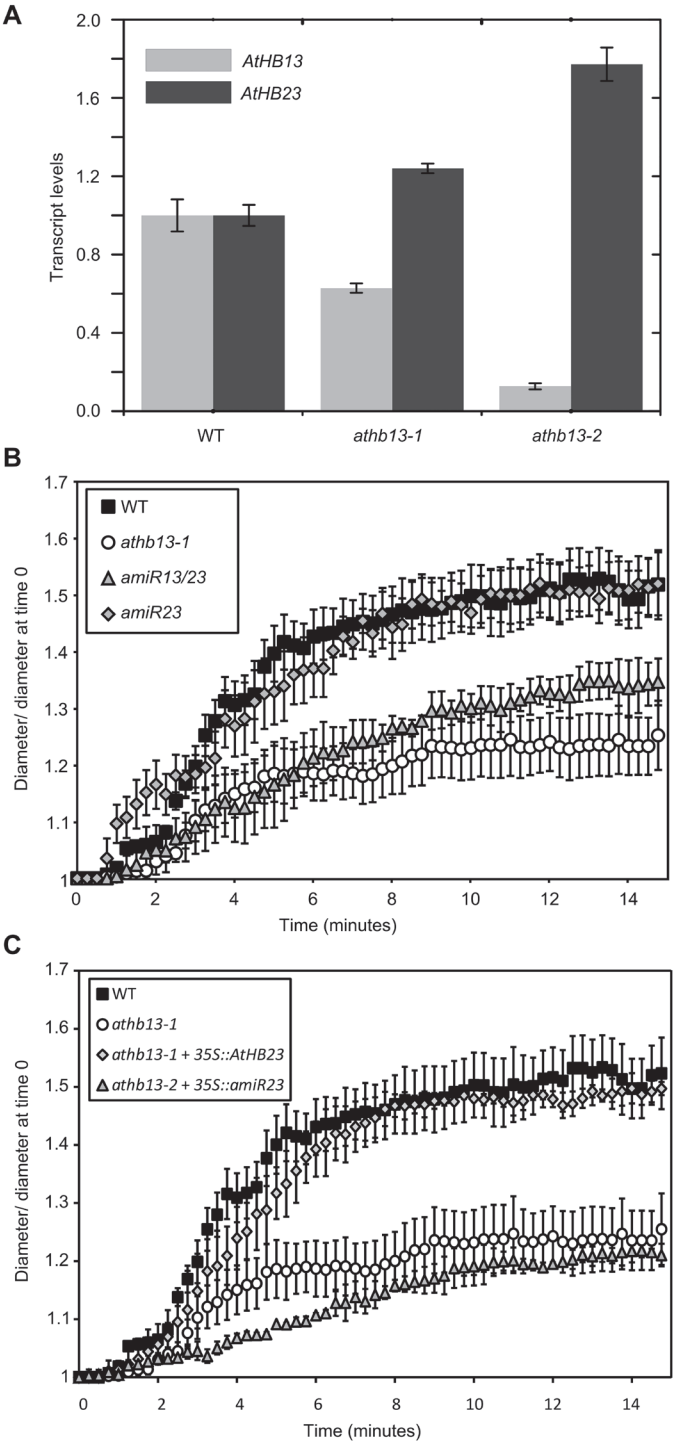

Fig. 8. *AtHB23* rescues abnormal phenotypes caused by *athb13-1* to obtain normal pollen hydration. (A) Relative transcript levels of *AtHB13* and *AtHB23* in WT, *athb13-1*, and *athb13-2* inflorescences. Transcript levels were normalized against WT transcripts by applying the $\Delta\Delta C_t$ method. Error bars represent standard error calculated from three independent biological replicates. Actin transcripts (*ACTIN2* and *ACTIN8*) were used as references. (B) Time course of pollen hydration on the stigmas of *athb13-1*, *amiRNA23*, and *amiRNA13/23* flowers that were artificially pollinated. (C) Time course of pollen hydration in WT, *athb13-1*, and *athb13-1* plants complemented with *35S::AtHB23* and *athb13-2* and transformed with *35S::amiR23*. In (B) and (C), images were captured every 15 s. The *y*-axis represents the relative diameter of the pollen grain with respect to its diameter at time 0. *n*=10 pollen grain per genotype. Bars represent standard deviation.

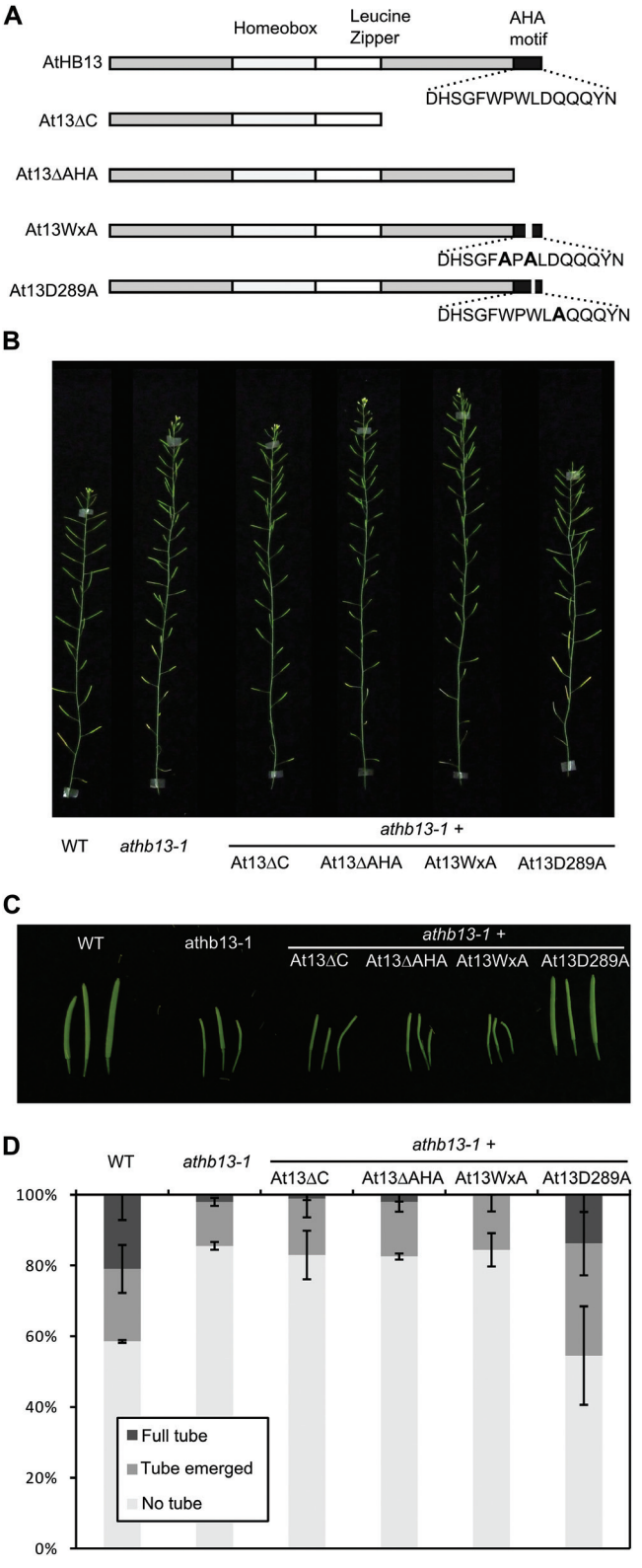

Fig. 9. The AtHB13 AHA motif is essential for its functionality. (A) Schematic representation of AtHB13 protein and the different variants that were used to complement the *athb13-1* abnormal phenotype (Capella *et al.*, 2014). (B) Representative photograph of *athb13-1* 35-d-old plants transformed with the constructs indicated in (A). (C) Representative photograph of siliques of the same genotypes. (D) *In vitro* pollen germination, 24 h after contact with pollen growth medium. *n*>250 pollen grains per genotype. Three independent lines for each genotype were analysed. Bars represent standard deviation.

entire C terminus or the AHA motif were deleted were not able to rescue either of the defective phenotypes. The same observation was made when both of the tryptophans present in the AHA motif were mutated to alanine, whereas a construct in which only aspartic acid 289 was mutated rescued the defect in a similar manner as WT AtHB13. These results indicated that the tryptophans that lie inside the AHA motif are essential for AtHB13 to accomplish its functions in inflorescence stem elongation and ovule fertilization.

Discussion

HD-Zip I AtHB13 has a crucial role in development

To date, only a limited number of HD-Zip I TFs have been related to developmental processes. In *Arabidopsis* LMI1 (Saddic *et al.*, 2006) and AtHB12 (Son *et al.*, 2010), HD-Zip I TFs have been described to be involved in flowering and stem development, respectively. Interesting examples of TFs from other plant species are garden pea TL (Hofer *et al.*, 2009) and barley VRS1 (Komatsuda *et al.*, 2007). The developmental roles of these TFs were discovered based on characterizations of mutant plants showing abnormal phenotypes. Moreover, in the latter cases, the mutations that helped to elucidate the roles of these TFs were found in the C termini of the proteins. In view of the importance of the relationship between conserved motifs in their C termini and the functional role of HD-Zip I TFs, AtHB13 appeared to be a very interesting candidate for further studies. This TF belongs to clade V and exhibits several motifs in its C terminus of unknown function that are shared with its apparent paralogue, AtHB23 (Arce *et al.*, 2011).

Evaluating *athb13-1* mutant plants during development in standard growth conditions allowed us to determine that serious abnormalities occurred in the reproductive stage. More precisely, stems grew faster and were higher at the end of the cycle, and siliques were clearly shorter, possessed fewer seeds, and had a large number of unfertilized ovules. This differential stem phenotype was due to faster growth of inflorescence stems in the segments between the upper internode and the inflorescence itself. The same phenotype was also evident in *athb13-2* mutant plants, which exhibited the insertion in a coding region, whereas defective siliques were observed only in *athb13-1* mutants. These observations were rather disconcerting, and the possibility of a second insertion in *athb13-1*, or in *athb13-2*, was discarded because the abnormal phenotypes were rescued (inflorescence stems for both mutants and siliques for *athb13-1*) after transforming the mutants with either *35S::AtHB13* or *35S::AtHB23*.

AtHB13 and its paralogue AtHB23 negatively affect inflorescence stem elongation

To understand the differential phenotype regarding inflorescence stem elongation, this trait was analysed in both of the *athb13* mutants and in the *athb23* and double *athb13/athb23* knockdown plants, as well as in mutants that were

transformed with *35S::AtHB13* or with *35S::AtHB23*. The results indicated that both AtHB13 and AtHB23 are independent negative regulators of elongation. Consistently, plants overexpressing the sunflower AtHB13 homologue, HaHB1, exhibited the opposite phenotype (i.e. a decrease in stem elongation rate) (Cabello *et al.*, 2012).

The faster elongation seems to be due to more active cell division rather than to differences in cell sizes (Fig. 5). Similar cell sizes were observed in mutant and WT stems, as well as upregulation of cyclins and unchanged transcript levels of genes involved in cell expansion (Somerville, 2006) in *athb13-1* mutants, both of which supported this idea (Fig. 5).

Notably, the differential inflorescence stem phenotype was presented by both *athb13* mutants and by *amiRNA23*, indicating that both apparent paralogue genes have roles in this developmental event. Because the mutation of either of these genes, as well as both of the genes, caused similar increases in stem growth rates, it is tempting to speculate that each one of them has specific targets or heterodimers that are required for their functions and therefore that the absence of one of them is sufficient to alter the phenotype. Such heterodimerization was proposed previously by Harris *et al.* (2011).

Role of AtHB13 in pollen hydration

Reproduction in *Arabidopsis* is accomplished after double fertilization between a female gametophyte and two male gametes. Pollination begins when desiccated pollen grains land on the stigma. This process includes fundamental events, and to achieve fertilization fine control of these steps is needed (Chapman and Goring, 2010).

Previous reports have indicated that both *AtHB13* and *AtHB23* are expressed in stigma and that *AtHB13* is also expressed in anthers (this work). Hence, it is tempting to speculate that these TFs could be involved in communication between pollen and stigma, in particular by playing a role in the generation of the pollen coat. Moreover, it has been suggested that molecules located on the extracellular surfaces of both pollen and stigma are responsible for such recognition (Edlund *et al.*, 2004). As shown in Supplementary Fig. S7 and Supplementary Table S1, a large number of the differentially expressed genes in *athb13-1* mutants are located in extracellular space. Among the genes that have previously been described as participating in pollen hydration, only *GRP17* was differentially expressed in *athb13-1* mutants (Mayfield and Preuss, 2000; Mayfield *et al.*, 2001; Updegraff *et al.*, 2009). Interestingly, of the 15 proteins that have been described as being expressed in *Arabidopsis* pollen coats, seven of them were repressed in *athb13-1* mutant plants to the same extent as *AtHB13* transcripts. Although the repression of these pollen coat genes was limited, the fact that a large proportion of these genes were downregulated could explain the observed phenotype. These observations could also explain the results that were obtained when pollen hydration of the *athb13-2* mutant was evaluated (Supplementary Fig. S5B). Certain *athb13-2* mutant pollen grains hydrated similarly to WT pollen grains, whereas others were similar to the *athb13-1* mutant. *AtHB13* is usually expressed in the tapetum (Fig. 3), which is the tissue that generates the pollen coat. From the tapetum, a heterogeneous substance is released that becomes the pollen coat, and in the pollen coat the pollen grain is imbibed before anthesis (Edlund *et al.*, 2004). It is possible that the natural complementation achieved by AtHB23 in the *athb13-2* mutant is not complete and therefore that select grains acquire a functional coat and others do not.

AtHB23 can substitute for AtHB13 in pollen when the latter is defective

With the aim of understanding why *athb13-1* and *athb13-2* plants exhibited such different siliques phenotypes, several experimental strategies were employed. *AtHB13* and *AtHB23* expression levels were evaluated in *athb13-1* and *athb13-2* plants, and the results were rather difficult to explain (Fig. 8A). Although the T-DNA insertion in the first mutant is located after the stop codon and inside the 3′ non-coding region, which enables almost complete transcription of the gene, several important events must be failing to progress because these plants demonstrated a highly abnormal phenotype. In the second mutant, the insertion is located inside of the coding region, specifically in the leucine zipper, and therefore it was expected to produce a more severe abnormal phenotype. However, this was not the case; on the contrary, *athb13-2* exhibited normal siliques, and differences were found only in inflorescence stems.

A recent report showed that the paralogues pair *AtHB12* and *AtHB7*, which are members of the HD-Zip I family, exhibits an interesting mechanism in which each member of the pair is able to affect the expression of the other (Ré *et al.*, 2014). This observation led us to propose that a similar phenomenon might be occurring with the pair *AtHB13*/*AtHB23*. A second potential explanation was that an incomplete AtHB13 protein was taking the place of the WT AtHB13 and therefore avoided the putative replacement function of AtHB23. Evaluation of *AtHB13* transcripts, both by RT-PCR and by RNA-Seq, corroborated that these transcripts were complete and were not partially degraded (Supplementary Fig. S6). Together with the absence of an abnormal silique phenotype in heterozygous plants (WT×*athb13-1*) or in WT plants transformed with the construct *35S::AtHB13ΔC* (Supplementary Fig. S6), this observation suggested that the first hypothesis was more likely to be correct: when the transcript levels of *AtHB13* are significantly reduced in siliques, *AtHB23* transcription (normally not expressed in this organ) is induced, and the resultant protein can substitute for the absence of AtHB13. Using specifically designed miRNAs, plants that were silenced at *AtHB23* and plants that were double silenced at *athb13*/*athb23* were generated and analysed. Notably, only *athb13-1* and the double-silenced construct led to the production of shorter siliques, whereas the remaining silenced genotypes led to a faster elongation rate of inflorescence stems (Fig. 4 and 8).

Because *AtHB23* knockdown plants did not exhibit abnormalities regarding their silique phenotypes or pollen hydration abilities, we concluded that the typical role of *AtHB23* is not related to pollen germination but is instead involved in a

bypass mechanism to prevent failures in plant reproduction. Moreover, although the expression patterns of *AtHB13* and *AtHB23* were similar in plants that were grown under normal conditions (Hanson *et al.*, 2002; Kim *et al.*, 2007), these genes are regulated by abscisic acid and salinity in nearly opposing manners (Henriksson *et al.*, 2005), indicating that they probably possess differential functions. Supporting this statement and according to RNA-Seq data, *AtHB13* transcript levels in WT plants were 5-fold those of *AtHB23* in inflorescences.

The question of how *AtHB23* senses the absence of functional *AtHB13* remains. We are currently unable to answer this question because *AtHB23* does not possess the pseudopalindromic CAATNATTG sequence that is bound by HD-Zip I proteins in its promoter region (Palena *et al.*, 1999; Johannesson *et al.*, 2001). It is tempting to speculate that one or more intermediary proteins act to transduce the signal. The results indicate an inverse relationship between transcript levels for *AtHB13* versus *AtHB23*, consistent with the idea that the transcript levels of the genes, and not protein levels, are being monitored. Our observations clearly indicated that a lack of *AtHB23* does not generate abnormal siliques and that siliques are shorter and pollen exhibits serious problems in germinating on stigma only when *AtHB13* is also absent. The characterization of the double knockdown corroborated these conclusions.

AHA motifs in AtHB13 are functionally essential

Interestingly, it could be demonstrated in this work that the C terminus of AtHB13 plays a crucial role in development. Although previous reports have indicated that the C terminus is essential for transactivation, the corresponding experiments were performed using artificial target genes (Capella *et al.*, 2014). On the other hand, AHA functionality *in planta* has been indirectly demonstrated for two different HD-Zip I TFs: VRS1 and TL (Komatsuda *et al.*, 2007; Hofer *et al.*, 2009). However, no experimental evidence regarding the importance of tryptophans in these AHA motifs has been reported previously. In this work, we showed that not only is the C terminus of AtHB13 functional but also that its AHA motif and tryptophans 285 and 287, which reside inside it, are essential.

Conclusions

To date, several *Arabidopsis* HD-Zip I mutants have been characterized, and the majority of previous reports have focused on their altered responses to illumination, environmental conditions, or hormone treatments (Aoyama *et al.*, 1995; Himmelbach *et al.*, 2002; Wang *et al.*, 2003; Manavella *et al.*, 2008; Barrero *et al.*, 2010; De Smet *et al.*, 2013); only a limited number of reports focusing on their roles in development have been published.

Here, we showed that *AtHB13* and *AtHB23* play negative roles in stem elongation and that *AtHB13* has a crucial function in pollen germination. When *AtHB13* was mutated, although its transcript levels were low, they were still detected by plant cells and led to an abnormal phenotype that was characterized by short siliques and unfertilized ovules. When there was an absence of available *AtHB13* transcripts in cells, *AtHB23*, which is an *AtHB13* paralogue, was somehow upregulated and could substitute for *AtHB13*.

Supplementary data

Supplementary data are available at *JXB* online.

Supplementary Fig. S1. The differential phenotype in stem lengths that is exhibited by *athb13-1* and *athb13*-2 mutants is rescued by AtHB13.

Supplementary Fig. S2. Expression of *AtHB13* and *AtHB23* in knockdown genotypes that were generated by transformation with amiRNAs.

Supplementary Fig. S3. Pollen tube development in pistils is impaired in *athb13-1* inflorescences.

Supplementary Fig. S4. Pollen adhesion is similar in *athb13-1* and WT plants.

Supplementary Fig. S5. Pollen hydration is defective in *athb13-2* mutant plants.

Supplementary Fig. S6. *AtHB13* transcript length is complete in *athb13*-1 mutants, and no evidence of a neomorphic AtHB13 protein was found.

Supplementary Fig. S7. RNA-seq results.

Supplementary Table S1. Genes differentially expressed in *athb13-1* inflorescences.

Supplementary Table S2. Genes differentially expressed in *athb13-1* inflorescences that are described as being involved in pollen hydration and germination.

Supplementary Table S3. Oligonucleotides used for cloning and RT-qPCR assays. Restriction sites are underlined.

Acknowledgements

This work was supported by the Agencia Nacional de Promoción Científica y Tecnológica (PICT 2011 0850 and PICT 2012 0955) and Universidad Nacional del Litoral (UNL). PR and MC are CONICET PhD Fellows. RLC is a CONICET Career member. The authors thank Dr Jorge Giacomelli for his help with RNA-Seq data and Dr Pablo Manavella for critical reading of the manuscript.

References

Aoyama T, Dong C, Wu Y, Carabelli M, Sessa G, Ruberti I, Morelli G, Chua N. 1995. Ectopic expression of the *Arabidopsis* transcriptional activator Athb-1 alters leaf cell fate in tobacco. *The Plant Cell* **7,** 1773–1785.

Arce AL, Raineri J, Capella M, Cabello JV, Chan RL. 2011. Uncharacterized conserved motifs outside the HD-Zip domain in HD-Zip subfamily I transcription factors; a potential source of functional diversity. *BMC Plant Biology* **11,** 42

Ariel FD, Manavella PA, Dezar CA, Chan RL. 2007. The true story of the HD-Zip family. *Trends in Plant Science* **12,** 419–426.

Barrero J, Millar A, Griffiths J, Czechowski T, Scheible W, Udvardi M, Reid J, Ross J, Jacobsen J, Gubler F. 2010. Gene expression profiling identifies two regulatory genes controlling dormancy and ABA sensitivity in *Arabidopsis* seeds. *The Plant Journal* **61,** 611–622.

Boavida LC, McCormick S. 2007. Temperature as a determinant factor for increased and reproducible *in vitro* pollen germination in *Arabidopsis thaliana*. *The Plant Journal* **52,** 570–582.

Bock KW, Honys D, Ward JM, Padmanaban S, Nawrocki EP, Hirschi KD, Twell D, Sze H. 2006. Integrating membrane transport with male

gametophyte development and function through transcriptomics. *Plant Physiology* **140,** 1151–1168.

Cabello JV, Arce AL, Chan RL. 2012. The homologous HD-Zip I transcription factors *HaHB1* and *AtHB13* confer cold tolerance via the induction of pathogenesis-related and glucanase proteins. *The Plant Journal* **69,** 141–153.

Cabello JV, Chan RL. 2012. The homologous homeodomain-leucine zipper transcription factors *HaHB1* and *AtHB13* confer tolerance to drought and salinity stresses via the induction of proteins that stabilize membranes. *Plant Biotechnology Journal* **10,** 815–825.

Capella M, Ré DA, Arce AL, Chan RL. 2014. Plant homeodomain-leucine zipper I transcription factors exhibit different functional AHA motifs that selectively interact with TBP or/and TFIIB. *Plant Cell Reports* **33,** 955–967.

Chapman LA, Goring DR. 2010. Pollen-pistil interactions regulating successful fertilization in the Brassicaceae. *Journal of Experimental Botany* **7,** 1987–1999.

Choi H, Jeong S, Kim D, Na H, Ryu J, Lee S, Nam H, Lim P, Woo H. 2014. The homeodomain-leucine zipper ATHB23, a phytochrome B-interacting protein, is important for phytochrome B-mediated red light signaling. *Physiologia Plantarum* **150,** 308–320.

Clough SJ, Bent AF. 1998. Floral dip: a simplified method for *Agrobacterium*-mediated transformation of *Arabidopsis thaliana*. *The Plant Journal* **16,** 735–743.

De Smet I, Lau S, Ehrismann J, Axiotis I, Kolb M, Kientz M, Wiejers D, Jürgens G. 2013. Transcriptional repression of *BODENLOS* by HD-ZIP transcription factor HB5 in *Arabidopsis thaliana*. *Journal of Experimental Botany* **64,** 3009–3019.

Dezar CA, Gago G, Gonzalez DH, Chan RL. 2005. *Hahb-4*, a sunflower homeobox-leucine zipper gene, is a developmental regulator and confers drought tolerance to *Arabidopsis thaliana* plants. *Transgenic Research* **14,** 429–440.

Edlund AF, Swanson R, Preuss D. 2004. Pollen and stigma structure and function: the role of diversity in pollination. *The Plant Cell* **16,** S84–S97.

Gao D, Appiano M, Huibers RP, Chen X, Loonen AEHM, Visser RGF, Wolters AMA, Bai Y. 2014. Activation tagging of *ATHB13* in *Arabidopsis thaliana* confers broad-spectrum disease resistance. *Plant Molecular Biology* **86,** 641–653.

Hanson J, Johannesson H, Engström P. 2001. Sugar-dependent alterations in cotyledon and leaf development in transgenic plants expressing the HDZhdip gene *ATHB13*. *Plant Molecular Biology* **45,** 247–262.

Hanson J, Regan S, Engström P. 2002. The expression pattern of the homeobox gene *ATHB13* reveals a conservation of transcriptional regulatory mechanisms between *Arabidopsis* and hybrid aspen. *Plant Cell Reports* **21,** 81–89.

Harris JC, Hrmova M, Lopato S, Langridge P. 2011. Modulation of plant growth by HD-Zip class I and II transcription factors in response to environmental stimuli. *New Phytologist* **190,** 823–837.

Henriksson E, Olsson A, Johannesson H, Johansson H, Hanson J, Engström P, Söderman E. 2005. Homeodomain leucine zipper class I genes in *Arabidopsis* expression patterns and phylogenetic relationships. *Plant Physiology* **139,** 509–518.

Himmelbach A, Hoffmann T, Leube M, Höhener B, Grill E. 2002. Homeodomain protein ATHB6 is a target of the protein phosphatase ABI1 and regulates hormone responses in *Arabidopsis*. *EMBO Journal* **21,** 3029–3038.

Hofer J, Turner L, Moreau C, *et al*. 2009. *Tendril-less* regulates tendril formation in pea leaves. *The Plant Cell* **21,** 420–428.

Jefferson RA, Kavanagh TA, Bevan MW. 1987. GUS fusions: β-glucuronidase as a sensitive and versatile gene fusion marker in higher plants. *EMBO Journal* **6,** 3901–3907.

Johannesson H, Wang Y, Engström P. 2001. DNA-binding and dimerization preferences of *Arabidopsis* homeodomain-leucine zipper transcription factors in vitro. *Plant Molecular Biology* **45,** 63–73.

Johannesson H, Wang Y, Hanson J, Engström P. 2003. The *Arabidopsis thaliana* homeobox gene *ATHB5* is a potential regulator of abscisic acid responsiveness in developing seedlings. *Plant Molecular Biology* **51,** 719–729.

Kim YK, Son O, Kim MR, Nam KH, Kim GT, Lee MS, Choi SY, Cheon CI. 2007. *AtHB23*, an *Arabidopsis* class I homeodomain-leucine zipper gene, is expressed in the adaxial region of young leaves. *Plant Cell Reports* **26,** 1179–1185.

Komarova NY, Thor K, Gubler A, Meier S, Dietrich D, Weichert A, Suter Grotemeyer M, Tegeder M, Rentsch D. 2008. AtPTR1 and AtPTR5 transport dipeptides in planta. *Plant Physiology* **148,** 856–869.

Komatsuda T, Pourkheirandish M, He C, *et al*. 2007. Six-rowed barley originated from a mutation in a homeodomain-leucine zipper I-class homeobox gene. *Proceedings of the National Academy of Sciences, USA* **104,** 1424–1429.

Lee YH, Oh HS, Cheon CI, Hwang IT, Kim YJ, Chun JY. 2001. Structure and expression of the *Arabidopsis thaliana* homeobox gene *Athb-12*. *Biochemical and Biophysical Research Communications* **284,** 133–141.

Li M, Bahn S-Ch, Guo L, Musgrave W, Berg H, Welti R, Wanga X. 2011. Patatin-related Phospholipase pPLAIIIb-induced changes in lipid metabolism alter cellulose content and cell elongation in *Arabidopsis*. *The Plant Cell* **23,** 1107–1123.

Loraine AE, McCormick S, Estrada A, Patel K, Qin P. 2013. RNA-Seq of *Arabidopsis* pollen uncovers novel transcription and alternative splicing. *Plant Physiology* **162,** 1092–1109.

Manavella P.A, Arce AL, Dezar CA, Bitton F, Renou J, Crespi M, Chan RL. 2006. Cross-talk between ethylene and drought signalling pathways is mediated by the sunflower Hahb-4 transcription factor. *The Plant Journal* **48,** 125–137.

Manavella PA, Dezar CA, Ariel FD, Drincovich MF, Chan RL. 2008. The sunflower HD-Zip transcription factor HaHB4 is up-regulated in darkness, reducing the transcription of photosynthesis-related genes. *Journal of Experimental Botany* **59,** 3143–3155.

Mayfield JA, Fiebig AF, Johnstone SE, Preuss D. 2001. Gene families from the *Arabidopsis thaliana* pollen coat proteome. *Science* **292,** 2482–2485.

Mayfield JA, Preuss D. 2000. Rapid initiation of *Arabidopsis* pollination requires the oleosin-domain protein GRP17. *Nature Cell Biology* **2,** 128–130.

Mitsuda N, Ohme-Takagi M. 2009. Functional analysis of transcription factors in *Arabidopsis*. *Plant and Cell Physiology* **50,** 1232–1248.

Mukherjee K, Brocchieri L, Bürglin TR. 2009. A comprehensive classification and evolutionary analysis of plant homeobox genes. *Molecular Biology Evolution* **26,** 2775–2794.

Olsson A, Engström P, Söderman E. 2004. The homeobox genes *ATHB12* and *ATHB7* encode potential regulators of growth in response to water deficit in *Arabidopsis*. *Plant Molecular Biology* **55,** 663–677.

Palena CM, Gonzalez DH, Chan RL. 1999. A monomer–dimer equilibrium modulates the interaction of the sunflower homeodomain leucine-zipper protein Hahb-4 with DNA. *Biochemical Journal* **341,** 81–87.

Ré DA, Capella M, Bonaventure G, Chan RL. 2014. *Arabidopsis* AtHB7 and AtHB12 evolved divergently to fine tune processes associated with growth and responses to water stress. *BMC Plant Biology* **14,** 150.

Ribichich KF, Arce AL, Chan RL. 2014. Coping with Drought and Salinity Stresses: The Role of Transcription Factors in Crop Improvement. In: Tuteja N, Gill SS, eds. *Climate change and plant abiotic stress tolerance*. Weinheim, Germany: Wiley-VCH, 641–684.

Riechmann JL, Heard J, Martin G, *et al*. 2000. *Arabidopsis* transcription factors: genome-wide comparative analysis among eukaryotes. *Science* **290,** 2105–2110.

Roeder AHK, Yanofsky MF. 2006. Fruit development in *Arabidopsis*. *The Arabidopsis Book* **4,** e0075.

Saddic L, Huvermann B, Bazhani S, Su Y, Winter C, Kwon C, Collum R, Wagner D. 2006. The LEAFY target LMI1 is a meristem identity regulator and acts together with LEAFY to regulate expression of *CAULIFLOWER*. *Development* **133,** 1673–1682.

Sakuma S, Pourkheirandish M, Hensel G, *et al*. 2013. Divergence of expression pattern contributed to neofunctionalization of duplicated HD-Zip I transcription factor in barley. *New Phytologist* **197,** 939–948.

Schwab R, Ossowski S, Riester M, Warthmann N, Weigel D. 2006. Highly specific gene silencing by artificial microRNAs in *Arabidopsis*. *The Plant Cell* **18,** 1121–1133.

Smyth DR, Bowman JL, Meyerowitz EM. 1990. Early flower development in *Arabidopsis. The Plant Cell* **2,** 755–767.

Somerville C. 2006. Cellulose synthesis in higher plants. *Annual Review of Cell and Developmental Biology* **22,** 53–78.

Son O, Hur YS, Kim YK, *et al*. 2010. ATHB12, an ABA-inducible homeodomain-leucine zipper (HD-Zip) protein of *Arabidopsis*, negatively regulates the growth of the inflorescence stem by decreasing the expression of a gibberellin 20-oxidase gene. *Plant and Cell Physiology* **51,** 1537–1547.

Updegraff EP, Zhao F, Preuss D. 2009. The extracellular lipase EXL4 is required for efficient hydration of *Arabidopsis* pollen. *Sex Plant Reproduction* **22,** 197–204.

Wang Y, Henriksson E, Söderman E, Henriksson K, Sundberg E, Engström P. 2003. The arabidopsis homeobox gene, *ATHB16*, regulates leaf development and the sensitivity to photoperiod in *Arabidopsis*. *Developmental Biology* **264,** 228–239.

Zhang S, Haider I, Kohlen W, Jiang L, Bouwmeester H, Meijer AH, Schluepmann H, Liu CM, Ouwerkerk PBF. 2012. Function of the HD-Zip I gene *Oshox22* in ABA-mediated drought and salt tolerances in rice. *Plant Molecular Biology* **80,** 571–585.

Figure S1

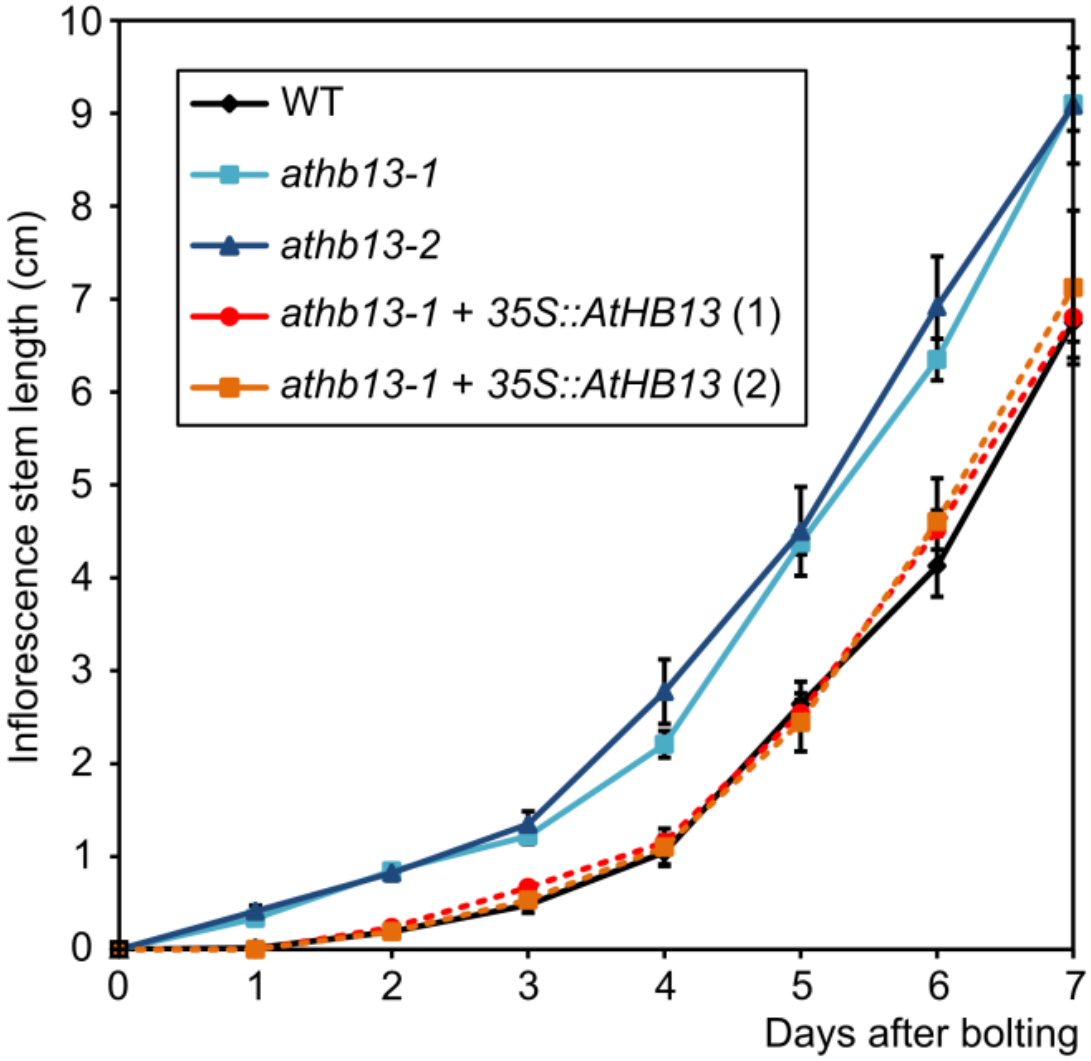

Figure S1. The differential phenotype in stem lengths that is exhibited by *athb13-1* and *athb13*-2 mutants is rescued by AtHB13. Kinetics of inflorescence stems elongation of WT, *athb13-1*, *athb13-2* and two independent lines of *athb13-1* transformed with *35S::AtHB13*. Time 0 corresponds to the day in which bolting was visualized. Inflorescence stems were measured with a ruler. Each point represents an average inflorescence stem length of 16 plants. Bars represent SE.

Figure S2

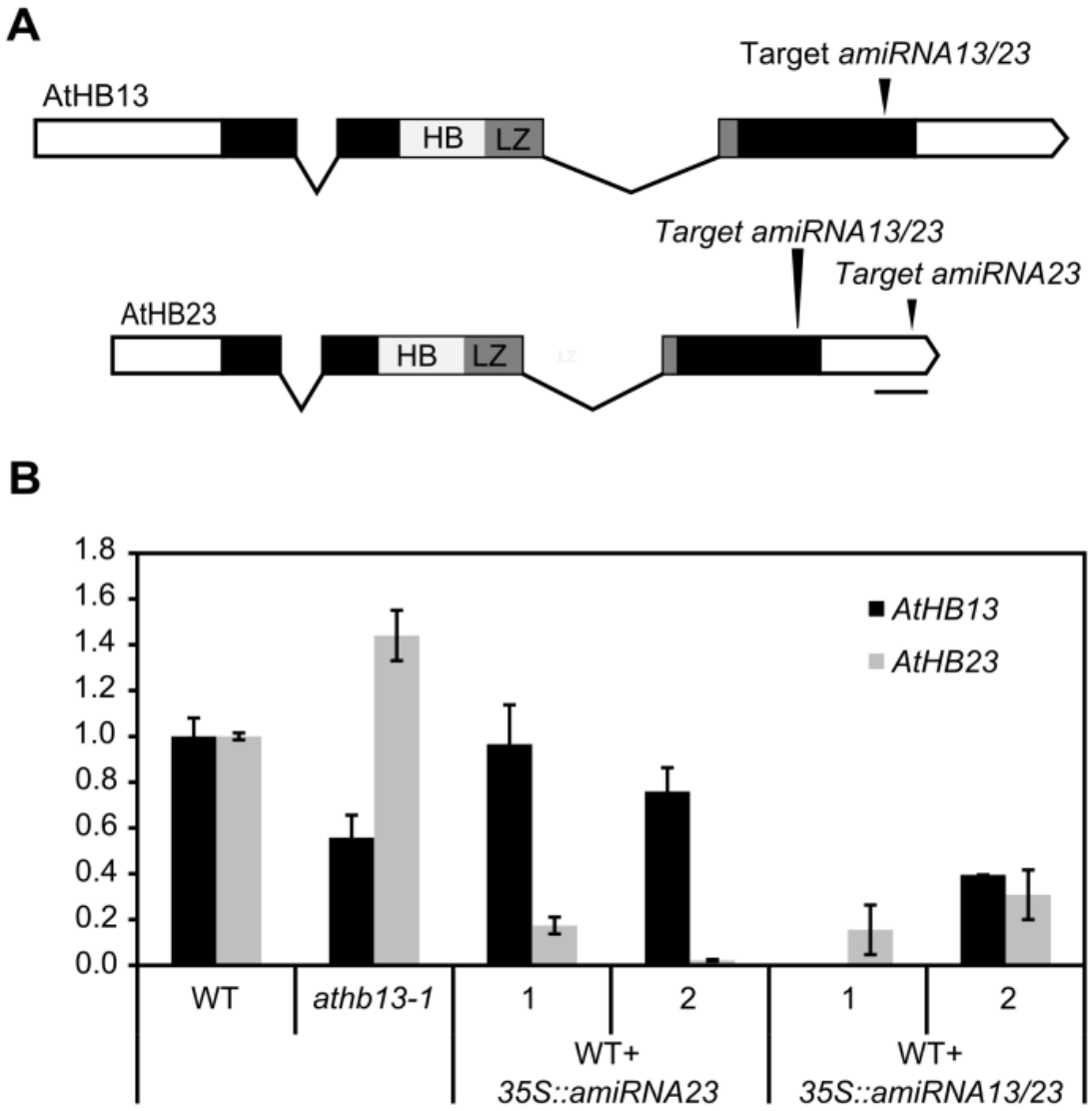

Fig. S2. Expression of *AtHB13* and *AtHB23* in knockdown genotypes that were generated by transformation with amiRNAs. (A) Schematic representation of *AtHB13* and *AtHB23* genes. White boxes represent 5' and 3' UTRs; filled boxes represent exons; lines represent introns. Arrowheads indicate the locations of amiRNA target sequences in each gene. HB: Homeobox, LZ: Leucine zipper. Scale bar: 100 bp. (B) Relative transcript levels of *AtHB13* and *AtHB23* in 35-day-old inflorescences analyzed by qRT-PCR. Transcript levels were normalized by applying the ΔΔCt method. Error bars represent SE calculated from three independent biological replicates. Actin transcripts (*ACTIN2* and *ACTIN8*) were used as references. The numbers 1 and 2 represent two independent lines of each genotype.

Figure S3

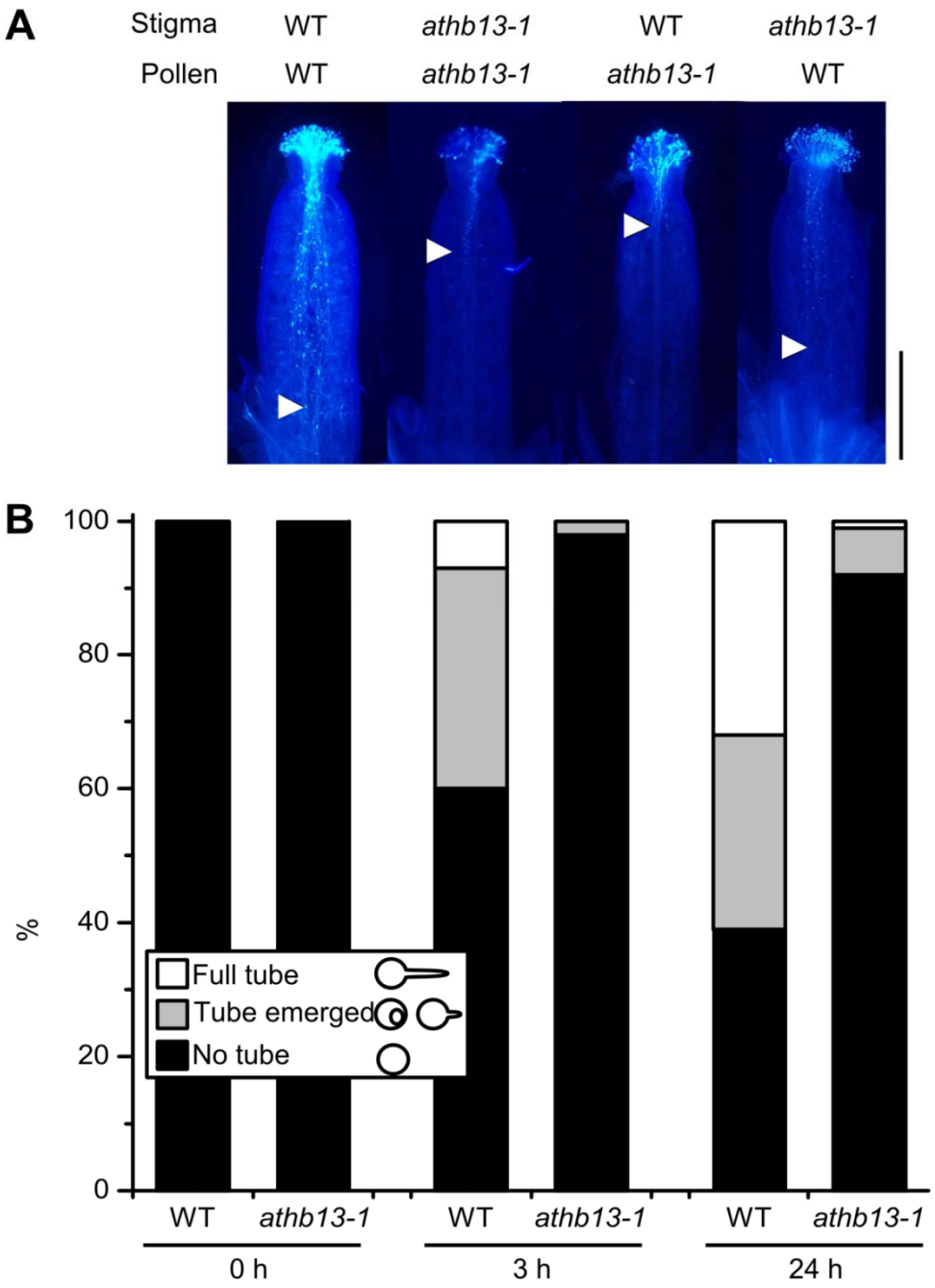

Fig. S3. Pollen tube development in pistils is impaired in *athb13-1* inflorescences. (A) Photographs of pollen grains of different genotype crosses as indicated in the top of each image. Pollen grains were aniline-blue stained and then visualized under epifluorescence microscopy; the photographs were taken 24 h after pollination. Arrows indicate the maximal lengths reached by the pollen tubes. Bar represents 500 µm. (B) Kinetics of pollen-tube emergence on solid media (n > 100 pollen grain of each genotype per time).

Figure S4

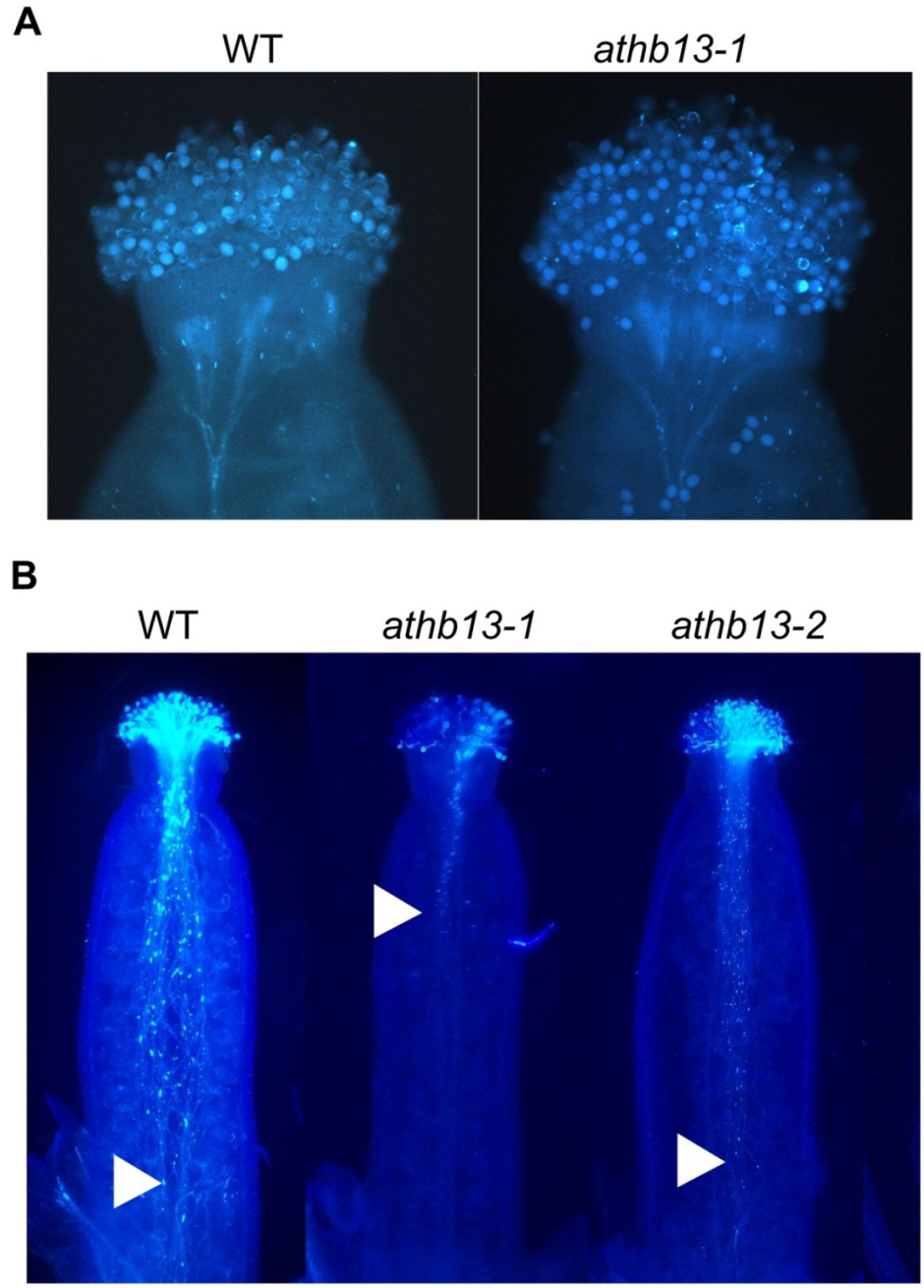

Fig. S4. Pollen adhesion is similar in *athb13-1* and WT plants. Non-pollinated pistils were artificially saturated with pollen grains and washed with 0.001 % Tween 20 in phosphate buffer. (B) Development of pollen tubes in pistils of WT, *athb13-1* and *athb13-2* mutant plants. Adhering pollen grains were visualized after staining with aniline blue under epifluorescence microscopy; the photographs were taken 24 hours after pollination. Arrows indicate the maximal length reached by the pollen tubes. The bar represents 500 μm.

Figure S5

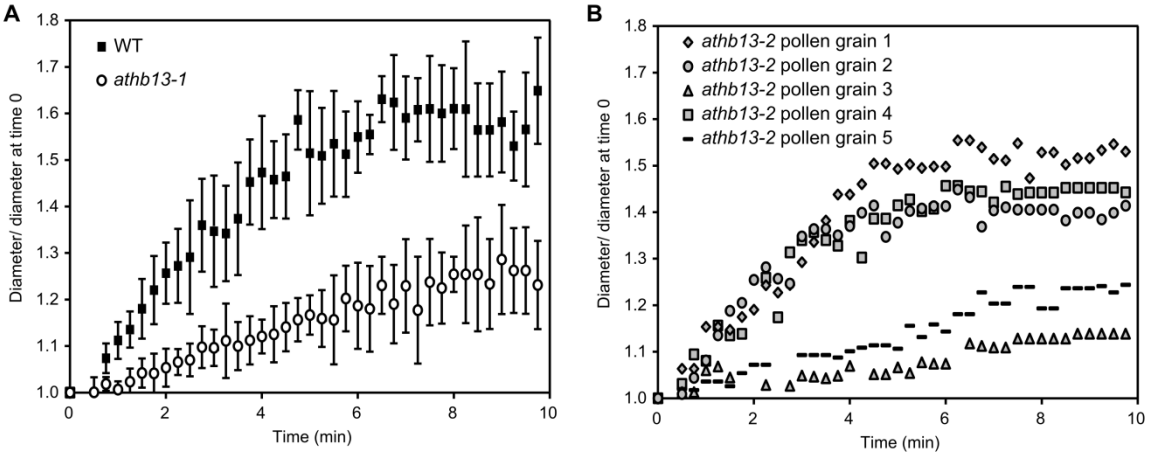

Figure S5. Pollen hydration is defective in *athb13-2* mutant plants. (A) Time course of pollen hydration on stigmas of *athb13-1* and WT plants. Flowers were tested at stage 12 (Smyth *et al*., 1990). Images were captured every 15 sec. Each point represents n = 10 pollen grains. Bars represent ± SD. (B) Time course of pollen hydration on stigmas for 5 different *athb13-2* pollen grains in the same pollination experiment. Flowers were tested at stage 12 (Smyth *et al*., 1990). Images were captured every 15 sec. Each point represents 1 pollen grain.

Figure S6

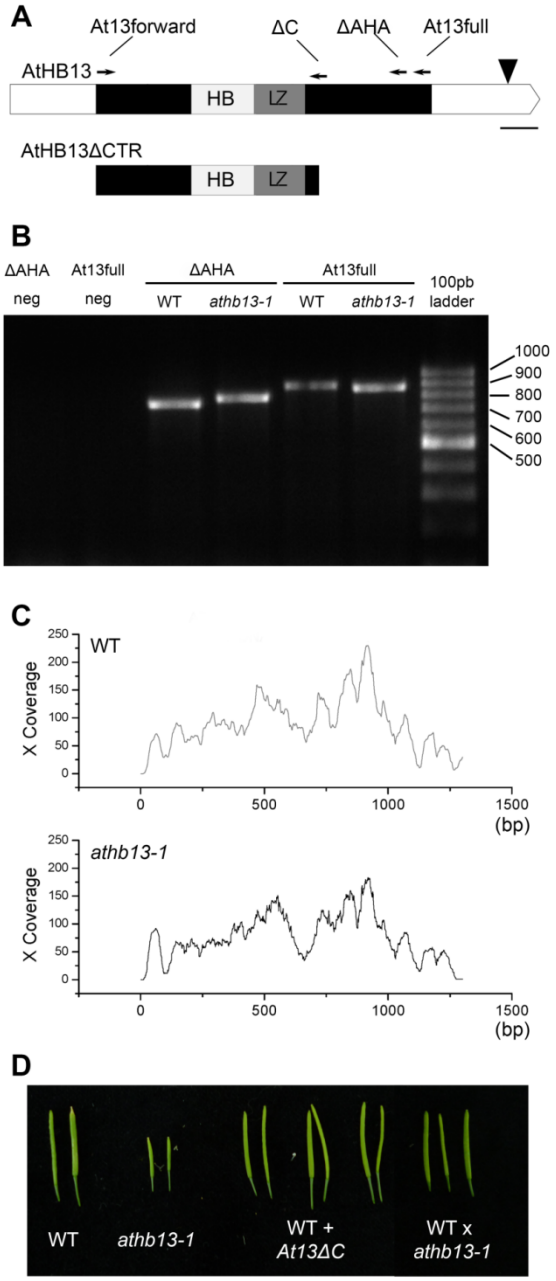

Figure S6. *AtHB13* transcript length is complete in *athb13*-1 mutants, and no evidence of a neomorphic AtHB13 protein was found. (A) *Upper panel*: schematic representation of the *AtHB13* gene showing the oligonucleotides that were used in PCR assays and the T-DNA insertion site; the bar represents 100 bp. *Lower panel*: Schematic representation of At13Δ*C* predicted protein. (B) RT-PCR products obtained from WT or mutant (*athb13-1*) RNAs with combinations of ΔAHA, At13forward and At13full oligonucleotides; negative controls were loaded into the first two lanes. (C) *AtHB13* transcript coverage in WT and *athb13-1* genotypes based on RNA-seq data. (D) Siliques of WT plants bearing the construct *35S::AtHB13*Δ*C* and heterozygous plants (obtained from crosses

between WT and *athb13-1)*. An intermediate phenotype was expected if a neomorphic AtHB13 protein was causing the defective phenotypes in *athb13-1* or WT+*35S::AtHB13*Δ*C* plants.

Figure S7

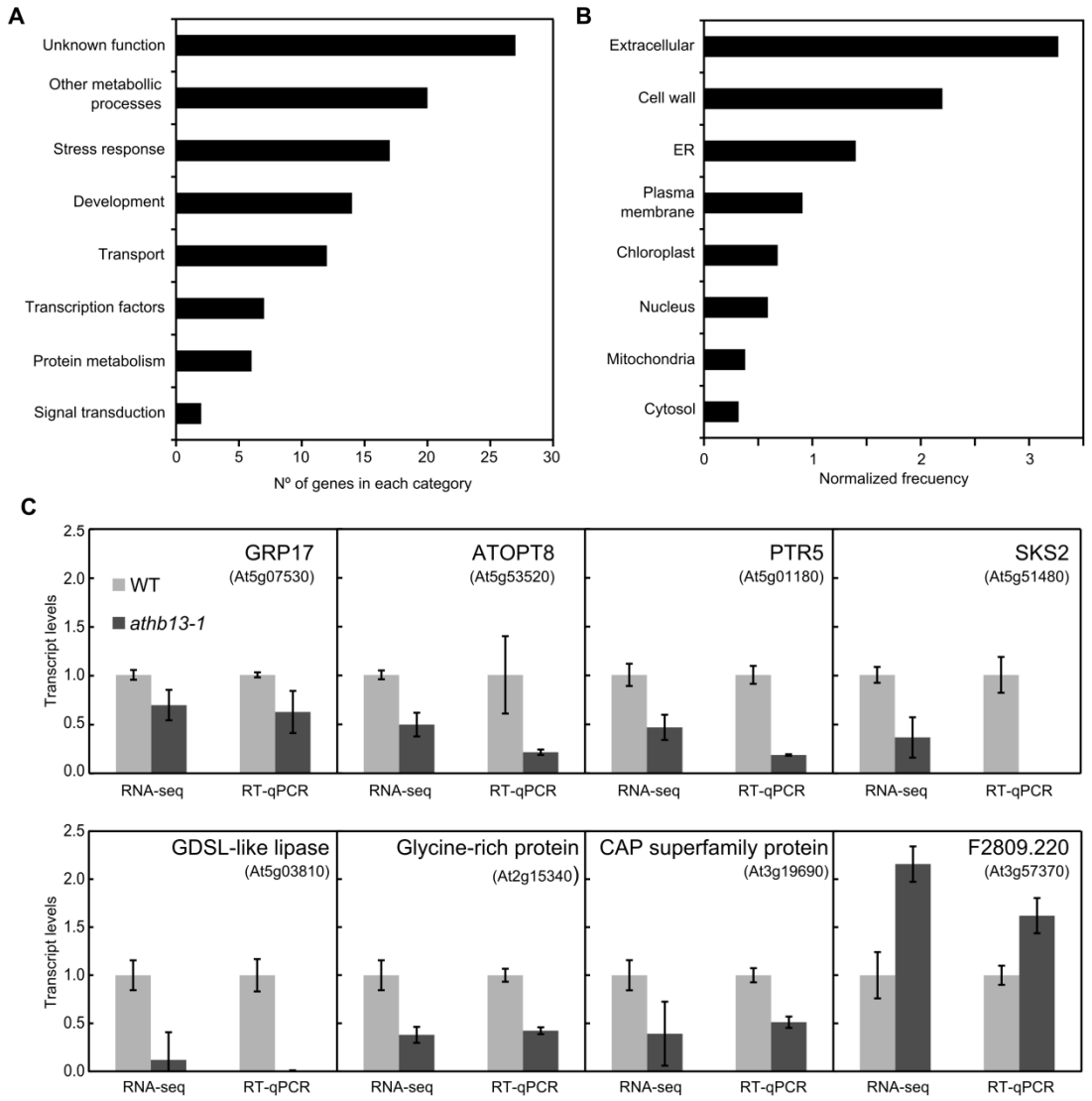

Figure S7. RNA-seq results. (A) Classification based on GO terms of differentially expressed genes in *athb13-1* inflorescences with respect to WT inflorescences. Classification was made using the BAR Classification Superviewer (http://bar.utoronto.ca/ntools/cgi-bin/ntools_classification_superviewer.cgi). (B) Sub-cellular localization of differentially expressed genes in athb13-1 inflorescences. Classification was made based on GO terms and using the BAR Classification Superviewer (http://bar.utoronto.ca/ntools/cgi-bin/ntools_classification_superviewer.cgi). (C) Transcript levels of differentially expressed genes in WT and *athb13-1* inflorescences. Transcript levels were normalized against WT transcripts by applying the ΔΔCt method. Error bars represent SE calculated from three independent biological replicates. *Actin* transcripts (*ACTIN2* and *ACTIN8*) were used as references. RNA-seq data represent average RPKM values from three independent biological replicates, which were normalized against

averaged WT RPKM. Error bars represent SE calculated from three independent biological replicates.

Table S1 Genes differentially expressed in *athb13-1* inflorescences.

Genes differentially expressed in a*thb13-1* versus WT inflorescences					
Gene ID	Protein name	Description	Fold change	Test T	HD-Zip Box
AT5G15360	F8M21_250	Protein of unknown function	219,000	0,000	
AT3G30383		Protein of unknown function (DUF784)	26,000	0,000	
AT5G48605		Putative membrane lipoprotein	20,000	0,000	
AT4G02850	T5J8.17	phenazine biosynthesis PhzC/PhzF family protein	6,500	0,001	CAATTATTG
AT1G57760		Protein of unknown function (DUF784)	5,800	0,004	
AT5G43525		Putative membrane lipoprotein	5,500	0,009	
AT5G42567		Protein of unknown function (DUF784)	5,300	0,005	
AT3G30247		Protein of unknown function (DUF784)	5,143	0,004	
AT2G21655		Protein of unknown function (DUF784)	5,125	0,001	
AT1G47470		Protein of unknown function (DUF784)	4,733	0,003	
AT5G18403		Putative membrane lipoprotein	4,250	0,008	
AT4G31710	ATGLR2.4	glutamate receptor 2.4	4,000	0,007	
AT2G21750	EC1.3	Protein of unknown function (DUF1278)	3,786	0,007	
AT3G01345		Expressed protein	3,400	0,000	
AT1G56385		Plant self-incompatibility protein S1 family	3,235	0,008	
AT1G57777		Protein of unknown function (DUF784)	3,231	0,000	
AT3G04510	LSH2	Protein of unknown function (DUF640)	3,200	0,001	
AT4G13263		Protein of unknown function (DUF784)	2,944	0,001	
AT2G04031		Protein of unknown function (DUF784)	2,875	0,003	
AT5G25970	T1N24.19	Core-2/I-branching beta-1,6-N-acetylglucosaminyltransferase family protein	2,810	0,004	
AT5G19880	PER58	Peroxidase superfamily protein	2,703	0,003	
AT2G21727		Protein of unknown function (DUF784)	2,667	0,004	
AT4G11290	PER39	Peroxidase superfamily protein	2,619	0,001	
AT1G47450		Protein of unknown function (DUF784)	2,611	0,003	
AT2G35640		Homeodomain-like superfamily protein	2,583	0,009	
AT3G03670	PER28	Peroxidase superfamily protein	2,558	0,000	
AT5G24900	CYP714A2	cytochrome P450, family 714, subfamily A, polypeptide 2	2,500	0,003	
AT3G27940	LBD26	LOB domain-containing protein 26	2,500	0,005	
AT5G11940	F14F18_110	Subtilase family protein	2,350	0,003	CAATTATTG
AT5G05300		Protein of unknown function	2,250	0,007	
AT1G27020	AT1G27020	Protein of unknown function	2,250	0,005	
AT5G55170	SUM3	small ubiquitin-like modifier 3	2,200	0,007	
AT3G11990	T21B14.17	Protein of unknown function (DUF784)	2,125	0,001	
AT5G05400		LRR and NB-ARC domains-containing disease resistance protein	2,067	0,008	
AT3G48080	T17F15.50	alpha/beta-Hydrolases superfamily protein	2,000	0,007	
AT1G15320	F9L1.26	Protein of unknown function	2,000	0,008	
AT3G26280	CYP71B4	cytochrome P450, family 71, subfamily B, polypeptide 4	0,500	0,007	
AT1G19190	CXE1	alpha/beta-Hydrolases superfamily protein	0,494	0,001	CAATTATTG
AT5G53520	ATOPT8	oligopeptide transporter 8	0,494	0,000	
AT5G51810	GA20OX2	gibberellin 20 oxidase 2	0,491	0,001	
AT2G22200	ERF056	Integrase-type DNA-binding superfamily protein	0,489	0,001	
AT1G29010		Protein of unknown function	0,488	0,005	
AT1G79840	GL2	HD-ZIP IV family of homeobox-leucine zipper protein with lipid-binding START domain	0,487	0,005	
AT3G30842	PDR10	pleiotropic drug resistance 10	0,486	0,009	
AT3G17230		invertase/pectin methylesterase inhibitor family protein	0,482	0,007	

AT3G14850	TBL41	TRICHOME BIREFRINGENCE-LIKE 41	0,482	0,003	
AT1G73620	F25P22.3	Pathogenesis-related thaumatin superfamily protein	0,480	0,000	
AT2G44480	BGLU17	beta glucosidase 17	0,479	0,005	
AT2G43620		Chitinase family protein	0,478	0,001	CAATAATTG
AT1G24540	CYP86C1	cytochrome P450, family 86, subfamily C, polypeptide 1	0,475	0,007	CAATAATTG
AT2G41230		Protein of unknown function	0,472	0,007	
AT4G37390	YDK1	Auxin-responsive GH3 family protein	0,468	0,003	
AT3G22820	EPFL5	allergen-related	0,468	0,007	CAATGATTG
AT5G01180	PTR5	peptide transporter 5	0,465	0,002	
AT1G23420	INO	Plant-specific transcription factor YABBY family protein	0,464	0,000	
AT5G41390		PLAC8 family protein	0,460	0,008	
AT5G04660	CYP77A4	cytochrome P450, family 77, subfamily A, polypeptide 4	0,456	0,001	
AT1G09790	COBL6	COBRA-like protein 6 precursor	0,442	0,004	
AT1G64940	CYP89A6	cytochrome P450, family 87, subfamily A, polypeptide 6	0,441	0,008	
AT1G34580	STP5	Major facilitator superfamily protein	0,441	0,004	
AT2G04046		Defensin-like (DEFL) family protein	0,438	0,003	
AT3G09450	F11F8_2	Protein of unknown function	0,438	0,000	
AT2G21465		Defensin-like (DEFL) family protein	0,436	0,002	CAATTATTG
AT1G04610	YUC3	YUCCA 3	0,434	0,001	
AT1G43640	AtTLP5	tubby like protein 5	0,434	0,006	
AT4G37770	ACS8	1-amino-cyclopropane-1-carboxylate synthase 8	0,433	0,008	
AT4G32490	ENODL4	early nodulin-like protein 4	0,429	0,006	
AT3G11740		Protein of unknown function (DUF567)	0,429	0,003	
AT5G01870	LTP10	Bifunctional inhibitor/lipid-transfer protein/seed storage 2S albumin superfamily protein	0,424	0,008	
AT4G32170	CYP96A2	cytochrome P450, family 96, subfamily A, polypeptide 2	0,421	0,000	
AT4G20390		Uncharacterised protein family (UPF0497)	0,420	0,003	
AT4G34550	T4L20.130	Protein of unknown function	0,418	0,002	
AT5G58782		Undecaprenyl pyrophosphate synthetase family protein	0,418	0,001	
AT5G58770		Undecaprenyl pyrophosphate synthetase family protein	0,414	0,004	
AT1G05990	RHS1	EF hand calcium-binding protein family	0,412	0,002	
AT5G52975		Protein of unknown function (DUF1278)	0,409	0,003	
AT3G60900	FLA10	FASCICLIN-like arabinogalactan-protein 10	0,407	0,004	
AT2G21320		B-box zinc finger family protein	0,406	0,000	
AT2G33750	ATPUP2	purine permease 2	0,403	0,001	
AT2G38860	YLS5	Class I glutamine amidotransferase-like superfamily protein	0,401	0,001	
AT3G19690		CAP (Cysteine-rich secretory proteins, Antigen 5, and Pathogenesis-related 1 protein) superfamily protein	0,391	0,007	
AT1G80820	CCR2	cinnamoyl coa reductase	0,383	0,001	
AT2G15340	AT2G15340	glycine-rich protein	0,379	0,002	
AT4G21440	ATMYB102	MYB-like 102	0,375	0,004	
AT3G59900	ARGOS	auxin-regulated gene involved in organ size	0,371	0,002	
AT5G61412		Protein of unknown function	0,370	0,009	
AT1G56650	PAP1	production of anthocyanin pigment 1	0,364	0,005	
AT5G51480	SKS2	SKU5 similar 2	0,363	0,001	
AT2G39200	MLO12	Seven transmembrane MLO family protein	0,357	0,010	
AT4G30074	LCR19	low-molecular-weight cysteine-rich 19	0,356	0,009	CAATTATTG
AT5G61730	ATATH11	ABC2 homolog 11	0,356	0,004	
AT4G36430	PER49	Peroxidase superfamily protein	0,353	0,002	

AT2G17690	SDC	F-box family protein with a domain of unknown function (DUF295)	0,353	0,004	
AT5G36910	THI2.2	thionin 2.2	0,353	0,000	
AT5G56300	GAMT2	gibberellic acid methyltransferase 2	0,352	0,008	
AT5G35550	TT2	Duplicated homeodomain-like superfamily protein	0,351	0,003	
AT1G06020		pfkB-like carbohydrate kinase family protein	0,342	0,009	
AT4G12960	GILT	Gamma interferon responsive lysosomal thiol (GILT) reductase family protein	0,336	0,001	
AT3G20520	SVL3	SHV3-like 3	0,332	0,002	
AT3G45060	ATNRT2.6	high affinity nitrate transporter 2.6	0,330	0,005	
AT5G48100	TT10	Laccase/Diphenol oxidase family protein	0,327	0,002	
AT3G22100	BHLH117	basic helix-loop-helix (bHLH) DNA-binding superfamily protein	0,327	0,004	
AT5G49180	PME58	Plant invertase/pectin methylesterase inhibitor superfamily	0,325	0,003	
AT5G33340	CDR1	Eukaryotic aspartyl protease family protein	0,324	0,008	
AT1G03495	3AT2	HXXXD-type acyl-transferase family protein	0,319	0,000	
AT5G17470	CML32	EF hand calcium-binding protein family	0,316	0,003	
AT1G70990	F15H11.18	proline-rich family protein	0,310	0,003	CAATCATTG
AT5G44390	K9L2.19	FAD-binding Berberine family protein	0,309	0,003	
AT1G59500	GH3.4	Auxin-responsive GH3 family protein	0,308	0,003	
AT2G02515		Protein of unknown function	0,304	0,009	
AT4G13840	F18A5.230	HXXXD-type acyl-transferase family protein	0,299	0,001	
AT2G03505		Carbohydrate-binding X8 domain superfamily protein	0,297	0,000	
AT5G22910	ATCHX9	cation/H+ exchanger 9	0,294	0,006	
AT5G17220	ATGSTF12	glutathione S-transferase phi 12	0,292	0,000	
AT1G73603	LCR64	low-molecular-weight cysteine-rich 64	0,288	0,002	
AT5G43610	ATSUC6	sucrose-proton symporter 6	0,286	0,000	
AT5G50200	WR3	nitrate transmembrane transporters	0,283	0,001	
AT3G49270		Protein of unknown function	0,282	0,000	
AT2G45840		Arabidopsis thaliana protein of unknown function (DUF821)	0,277	0,004	
AT5G55132		Defensin-like (DEFL) family protein	0,276	0,002	
AT5G62040	BFT	PEBP (phosphatidylethanolamine-binding protein) family protein	0,273	0,001	CAATAATTG
AT4G09820	TT8	basic helix-loop-helix (bHLH) DNA-binding superfamily protein	0,269	0,007	
AT1G02550		Plant invertase/pectin methylesterase inhibitor superfamily protein	0,267	0,009	
AT5G46950		Plant invertase/pectin methylesterase inhibitor superfamily protein	0,264	0,004	
AT2G43590		Chitinase family protein	0,257	0,001	CAATCATTG
AT2G23148		Plant self-incompatibility protein S1 family	0,256	0,008	
AT1G14455	F14L17.23	Protein of unknown function	0,254	0,000	
AT3G29034		Protein of unknown function	0,250	0,000	CAATAATTG
AT2G39855	T5I7.3	Protein of unknown function	0,250	0,000	
AT1G03020	GRXS1	Thioredoxin superfamily protein	0,250	0,006	
AT1G32763		Cysteine-rich protein	0,250	0,001	
AT4G23360		Protein of unknown function	0,250	0,007	
AT4G02520	ATGSTF2	glutathione S-transferase PHI 2	0,248	0,000	
AT1G30730	T5I8.18	FAD-binding Berberine family protein	0,247	0,002	
AT1G03940	3AT1	HXXXD-type acyl-transferase family protein	0,245	0,000	
AT2G37260	TTG2	WRKY family transcription factor family protein	0,242	0,001	
AT3G21500	DXPS1	1-deoxy-D-xylulose 5-phosphate synthase 1	0,242	0,004	
AT1G77525		Protein of unknown function	0,241	0,000	
AT2G46660	CYP78A6	cytochrome P450, family 78, subfamily A, polypeptide 6	0,240	0,000	
AT1G44130	T7O23.17	Eukaryotic aspartyl protease family protein	0,238	0,004	CAATCATTG

AT3G24510		Defensin-like (DEFL) family protein	0,237	0,003	
AT1G61255	F11P17.3	Protein of unknown function	0,234	0,002	
AT1G13755		Defensin-like (DEFL) family protein	0,234	0,003	
AT2G35980	YLS9	Late embryogenesis abundant (LEA) hydroxyproline-rich glycoprotein family	0,233	0,000	CAATGATTG
AT1G02930	GSTF6	glutathione S-transferase 6	0,233	0,001	
AT3G48230	T24C20_110	Protein of Unknown Function (DUF239)	0,232	0,002	
AT5G63087		Plant thionin family protein	0,231	0,000	
AT5G63085		Plant thionin family protein	0,229	0,004	
AT1G21470		Protein of unknown function	0,227	0,004	
AT5G24110	WRKY30	WRKY DNA-binding protein 30	0,226	0,002	
AT5G39580	PER62	Peroxidase superfamily protein	0,226	0,002	
AT4G14090	UGT75C1	UDP-Glycosyltransferase superfamily protein	0,226	0,000	
AT3G48231	LCR48	low-molecular-weight cysteine-rich 48	0,226	0,003	
AT1G15040	AT1G15045	Class I glutamine amidotransferase-like superfamily protein	0,226	0,002	
AT3G05975		Late embryogenesis abundant (LEA) hydroxyproline-rich glycoprotein family	0,222	0,006	
AT1G34790	TT1	C2H2 and C2HC zinc fingers superfamily protein	0,221	0,008	
AT3G57250	F28O9.100	Emsy N Terminus (ENT) domain-containing protein	0,219	0,008	CAATAATTG
AT3G09270	ATGSTU8	glutathione S-transferase TAU 8	0,214	0,005	
AT1G04645	T1G11.10	Plant self-incompatibility protein S1 family	0,214	0,001	
AT5G42830		HXXXD-type acyl-transferase family protein	0,213	0,000	
AT3G05460	F22F7.9	sporozoite surface protein-related	0,211	0,002	
AT3G61172	LCR8	low-molecular-weight cysteine-rich 8	0,211	0,006	
AT4G33820	AT4G33820	Glycosyl hydrolase superfamily protein	0,211	0,006	
AT3G29590	AT5MAT	HXXXD-type acyl-transferase family protein	0,206	0,000	
AT2G27320		Protein of Unknown Function (DUF239)	0,200	0,008	
AT3G04300	T6K12.8	RmlC-like cupins superfamily protein	0,200	0,003	
AT5G46300		Protein of unknown function	0,200	0,000	
AT2G18880	VEL2	vernalization5/VIN3-like	0,200	0,005	
AT3G03828		Protein of unknown function	0,198	0,000	
AT2G23990	ENODL11	early nodulin-like protein 11	0,195	0,005	
AT1G17260	AHA10	autoinhibited H(+)-ATPase isoform 10	0,194	0,009	
AT4G37720	ATPSK6	phytosulfokine 6 precursor	0,188	0,008	CAATAATTG
AT1G78710	TBL42	TRICHOME BIREFRINGENCE-LIKE 42	0,183	0,001	
AT1G56415		Expressed protein	0,182	0,000	
AT2G39518		Uncharacterised protein family (UPF0497)	0,182	0,001	
AT3G17600	IAA31	indole-3-acetic acid inducible 31	0,178	0,002	
AT3G17152		Plant invertase/pectin methylesterase inhibitor superfamily protein	0,176	0,006	
AT3G16660	MGL6_11	Pollen Ole e 1 allergen and extensin family protein	0,176	0,004	
AT4G02300	PME39	Plant invertase/pectin methylesterase inhibitor superfamily	0,174	0,000	
AT1G62333		Protein of unknown function	0,170	0,004	
AT1G73610		GDSL-like Lipase/Acylhydrolase superfamily protein	0,168	0,003	
AT2G33780	T1B8.28	VQ motif-containing protein	0,167	0,006	CAATGATTG
AT4G29033		Defensin-like (DEFL) family protein	0,167	0,007	CAATTATTG
AT5G44360		FAD-binding Berberine family protein	0,167	0,001	
AT3G13010		hAT transposon superfamily protein	0,167	0,007	
AT5G11412		RNA-binding (RRM/RBD/RNP motifs) family protein	0,167	0,007	
AT5G09370	T5E8_170	Bifunctional inhibitor/lipid-transfer protein/seed storage 2S albumin superfamily protein	0,166	0,000	
AT5G54060	UF3GT	UDP-glucose:flavonoid 3-o-glucosyltransferase	0,165	0,000	
AT2G46960	CYP709B1	cytochrome P450, family 709, subfamily B, polypeptide 1	0,163	0,005	
AT3G59030	TT12	MATE efflux family protein	0,161	0,003	

AT5G63170		GDSL-like Lipase/Acylhydrolase superfamily protein	0,160	0,001	
AT1G58055		Defensin-like (DEFL) family protein	0,151	0,001	
AT5G48905	LCR12	low-molecular-weight cysteine-rich 12	0,151	0,009	CAATTATTG
AT2G32370	HDG3	homeodomain GLABROUS 3	0,149	0,004	
AT4G33585		Protein of unknown function	0,147	0,000	
AT4G23350	F16G20.50	Protein of Unknown Function (DUF239)	0,144	0,004	
AT3G55665		Plant self-incompatibility protein S1 family	0,143	0,003	
AT5G27238		Plant self-incompatibility protein S1 family	0,139	0,009	
AT4G19905	LCR38	low-molecular-weight cysteine-rich 38	0,137	0,003	
AT1G16390	ATOCT3	organic cation/carnitine transporter 3	0,134	0,001	
AT2G22060	T16B14.9	Protein of unknown function	0,133	0,003	
AT1G24000		Polyketide cyclase/dehydrase and lipid transport superfamily protein	0,133	0,003	
AT3G25280		Major facilitator superfamily protein	0,125	0,008	
AT5G58850	ATMYB119	myb domain protein 119	0,125	0,008	
AT2G43000	anac042	NAC domain containing protein 42	0,125	0,001	
AT1G09370	F14J9.3	Plant invertase/pectin methylesterase inhibitor superfamily protein	0,125	0,000	
AT5G64905	PROPEP3	elicitor peptide 3 precursor	0,121	0,005	CAATCATTG
AT1G64830	F13O11.13	Eukaryotic aspartyl protease family protein	0,120	0,002	
AT1G02920	ATGSTF7	glutathione S-transferase 7	0,118	0,000	
AT5G03810		GDSL-like Lipase/Acylhydrolase family protein	0,118	0,001	
AT1G51920		Protein of unknown function	0,118	0,006	
AT4G22880	LDOX	leucoanthocyanidin dioxygenase	0,115	0,000	
AT5G51105		Protein of unknown function (DUF1278)	0,115	0,001	
AT2G04910		Carbohydrate-binding X8 domain superfamily protein	0,113	0,001	
AT1G26510		F-box associated ubiquitination effector family protein	0,111	0,001	CAATTATTG
AT4G32105		Beta-1,3-N-Acetylglucosaminyltransferase family protein	0,110	0,004	
AT1G56100		Plant invertase/pectin methylesterase inhibitor superfamily protein	0,110	0,002	
AT1G31250		proline-rich family protein	0,101	0,007	
AT1G61720	BAN	NAD(P)-binding Rossmann-fold superfamily protein	0,101	0,005	
AT5G48945	LCR46	low-molecular-weight cysteine-rich 46	0,100	0,000	CAATAATTG
AT2G31083	CLE5	CLAVATA3/ESR-RELATED 5	0,100	0,001	
AT3G02670	F16B3.30	Glycine-rich protein family	0,100	0,002	
AT1G02360	T6A9.5	Chitinase family protein	0,094	0,008	
AT5G56369		Defensin-like (DEFL) family protein	0,091	0,002	
AT5G58840		Subtilase family protein	0,091	0,000	
AT5G42800	DFR	dihydroflavonol 4-reductase	0,090	0,000	
AT5G54220		Cysteine-rich protein	0,087	0,007	CAATAATTG
AT4G29285	LCR24	low-molecular-weight cysteine-rich 24	0,087	0,002	
AT2G04032	ZIP7	zinc transporter 7 precursor	0,087	0,001	
AT4G33840	F17I5.30	Glycosyl hydrolase family 10 protein	0,086	0,008	
AT5G07850	F13G24.50	HXXXD-type acyl-transferase family protein	0,086	0,007	
AT4G30070	LCR59	low-molecular-weight cysteine-rich 59	0,083	0,006	
AT5G46877		Defensin-like (DEFL) family protein	0,083	0,005	
AT5G46040	PTR3-B	Major facilitator superfamily protein	0,083	0,001	
AT2G38900		Serine protease inhibitor, potato inhibitor I-type family protein	0,075	0,001	
AT2G20208	LCR60	low-molecular-weight cysteine-rich 60	0,073	0,000	
AT2G30750	CYP71A12	cytochrome P450, family 71, subfamily A, polypeptide 12	0,072	0,001	
AT2G30810	GASA12	Gibberellin-regulated family protein	0,071	0,000	
AT5G10230	ANNAT7	annexin 7	0,071	0,000	

AT4G15750	DL3915C	Plant invertase/pectin methylesterase inhibitor superfamily protein	0,069	0,001	
AT3G04280	ARR22	response regulator 22	0,067	0,006	
AT1G24062		Cysteine-rich protein	0,067	0,000	
AT4G19035	LCR7	low-molecular-weight cysteine-rich 7	0,067	0,002	
AT3G03260	HDG8	homeodomain GLABROUS 8	0,065	0,001	
AT5G39130		RmlC-like cupins superfamily protein	0,063	0,006	
AT3G05741		Plant invertase/pectin methylesterase inhibitor superfamily protein	0,063	0,001	
AT2G39640		glycosyl hydrolase family 17 protein	0,061	0,002	
AT2G26865		Encodes a Plant thionin family protein	0,061	0,001	
AT5G58820		Subtilisin-like serine endopeptidase family protein	0,059	0,001	
AT5G47350		alpha/beta-Hydrolases superfamily protein	0,059	0,003	
AT4G30064	LCR61	low-molecular-weight cysteine-rich 61	0,059	0,000	
AT5G38195		Bifunctional inhibitor/lipid-transfer protein/seed storage 2S albumin superfamily protein	0,059	0,005	
AT3G55677		Plant self-incompatibility protein S1 family	0,059	0,001	
AT1G13609		Defensin-like (DEFL) family protein	0,058	0,001	
AT1G26380	T1K7.24	FAD-binding Berberine family protein	0,057	0,009	
AT4G13095	LCR37	low-molecular-weight cysteine-rich 37	0,057	0,007	
AT4G35725		Protein of unknown function	0,056	0,000	
AT4G22115	SCRL14	SCR-like 14	0,056	0,009	
AT4G15735	SCRL10	SCR-like 10	0,053	0,000	
AT1G64107		Putative membrane lipoprotein	0,053	0,005	
AT2G44240		Protein of Unknown Function (DUF239)	0,050	0,000	
AT1G21850	sks8	SKU5 similar 8	0,050	0,002	
AT5G39300	ATEXPA25	expansin A25	0,048	0,000	
AT1G13605		Encodes a defensin-like (DEFL) family protein.	0,045	0,000	
AT1G26390	T1K7.23	FAD-binding Berberine family protein	0,043	0,008	
AT5G53100		NAD(P)-binding Rossmann-fold superfamily protein	0,043	0,001	
AT3G25420	scpl21	serine carboxypeptidase-like 21	0,043	0,000	
AT2G47115		Protein of unknown function	0,042	0,001	
AT2G02147	LCR73	low-molecular-weight cysteine-rich 73	0,041	0,005	
AT5G54225	LCR83	low-molecular-weight cysteine-rich 83	0,037	0,000	
AT3G01324		ECA1-like gametogenesis related family protein	0,032	0,006	
AT3G27425		ECA1-like gametogenesis related family protein	0,031	0,000	
AT1G61688		Defensin-like (DEFL) family protein	0,029	0,002	
AT2G31953	LCR76	low-molecular-weight cysteine-rich 76	0,026	0,000	CAATGATTG
AT3G29570		Protein of unknown function	0,022	0,002	
AT1G63057		Protein of unknown function	0,021	0,004	
AT2G44540	AtGH9B9	glycosyl hydrolase 9B9	0,019	0,001	
AT2G14365	LCR84	low-molecular-weight cysteine-rich 84	0,017	0,000	
AT4G13080	XTH1	xyloglucan endotransglucosylase/hydrolase 1	0,015	0,004	
AT1G63055		Protein of unknown function	0,011	0,001	
AT5G39280	ATEXPA23	expansin A23	0,009	0,000	
AT1G12665		Encodes a Plant thionin family protein	0,008	0,000	
AT4G17710	HDG4	homeodomain GLABROUS 4	0,000	0,001	CAATAATTG
AT1G29962	AGL64	AGAMOUS-like 64	0,000	0,002	CAATCATTG
AT2G21110		Disease resistance-responsive (dirigent-like protein) family protein	0,000	0,000	
AT2G44550	AtGH9B10	glycosyl hydrolase 9B10	0,000	0,000	
AT4G14630	GLP9	germin-like protein 9	0,000	0,007	
AT1G74045	TET17	tetraspanin 17	0,000	0,007	
AT4G30380	EGC1	Barwin-related endoglucanase	0,000	0,004	
AT5G53780		Protein of unknown function (DUF295)	0,000	0,007	
AT5G13620		Protein of unknown function	0,000	0,001	
AT2G25685	SCRL17	SCR-like 17	0,000	0,002	

AT5G53610		Carbohydrate-binding X8 domain superfamily protein	0,000	0,001
AT5G63230		Carbohydrate-binding X8 domain superfamily protein	0,000	0,007
AT5G51845		Defensin-like (DEFL) family protein	0,000	0,007
AT5G59105		Defensin-like (DEFL) family protein	0,000	0,007
AT2G36180	CML31	EF hand calcium-binding protein family	0,000	0,002
AT5G56390		F-box/RNI-like/FBD-like domains-containing protein	0,000	0,007
AT1G80330	ATGA3OX4	gibberellin 3-oxidase 4	0,000	0,002
AT4G09795	LCR13	low-molecular-weight cysteine-rich 13	0,000	0,007
AT2G04425	LCR82	low-molecular-weight cysteine-rich 82	0,000	0,007
AT1G17150		Pectin lyase-like superfamily protein	0,000	0,007
AT3G01880	F1C9.34	Plant protein of unknown function (DUF946)	0,000	0,007
AT5G06020		Plant self-incompatibility protein S1 family	0,000	0,007
AT1G13520	AT1G13520	Protein of unknown function (DUF1262)	0,000	0,001
AT4G23080	F7H19.270	Protein of Unknown Function (DUF239)	0,000	0,004
AT2G25305		Putative membrane lipoprotein	0,000	0,002
AT1G23145	RALFL2	RALF-like 2	0,000	0,000
AT4G22400	AT4G22400	Protein of unknown function	0,000	0,007
AT3G49770	T16K5.120	Protein of unknown function	0,000	0,007

Table S2 Genes differentially expressed in *athb13-1* inflorescences that are described as being involved in pollen hydration and germination.

Genes involved in pollen hydration and germination				
Locus	Name	Description	Fold change	T-Test
Cell wall modifiers				
AT5G35390	RLK	Leucine-rich repeat protein kinase family protein	0,1961	0,0002
AT2G15340		Glycine-rich protein	0,3789	0,0025
AT3G03080	T17B22.23	Zinc-binding dehydrogenase family protein	0,5490	0,0002
AT1G79400	ATCHX2	Cation/H+ exchanger 2	0,5409	0,0018
AT2G20430	RIC6	ROP-interactive CRIB motif-containing protein 6	0,5875	0,0009
AT2G33670	MLO5	Seven transmembrane MLO family protein	0,5382	0,0011
AT1G04450	RIC3	ROP-interactive CRIB motif-containing protein 3	0,6231	0,0037
AT4G31230		Protein kinase protein with adenine nucleotide alpha hydrolases-like domain	0,6300	0,0061
AT4G03620	T5L23.11	Myosin heavy chain-related	0,6719	0,0083
AT1G69940	ATPPME1	Pectin lyase-like superfamily protein	0,6907	0,0007
AT5G07510	GRP14	Glycine-rich protein 14	0,6955	0,0182
Transporters				
AT5G01180	PTR5	Peptide transporter 5	0,4976	0,0100
AT5G53520	ATOPT8	Oligopeptide transporter 8	0,4935	0,0003
AT1G12090		Extensin-like protein	0,6777	0,0173
Transcription factors				
AT5G54470		B-box type zinc finger family protein	0,4436	0,0000
AT5G47370	HAT2	Homeobox-leucine zipper protein 4 (HB-4) / HD-ZIP protein	0,6349	0,0009
AT4G09960	STK	K-box region and MADS-box transcription factor family protein	0,5173	3,2E-05
AT5G39860	PRE1	Basic helix-loop-helix (bHLH) DNA-binding family protein	0,4862	0,0169
Otros				
AT1G24620	CML25	EF hand calcium-binding protein family	0,6122	0,0144
AT5G07530	GRP17	Glycine rich protein 17	0,6836	0,0343

Table S3 Oligonucleotides used for cloning and qRT-PCR assays. Restriction sites are underlined.

Oligonucleotide Name	Sequence	Restriction Site	Construct/Uses
AtHB13q F	CTCCATGGATTTGCTTCG		Quantification by RT-qPCR
AtHB13q R	TCCCATTTGTGACCCATC		Quantification by RT-qPCR
At13forward	GGCTCTAGAATGTCTTGTAATAATGGAATGTC	XbaI	RT-PCR / AtHB13 cloning
At13full	GCCGGATCCATTTCAATTGTACTGTTGCTGATC	BamHI	RT-PCR
AtHB13 ΔAHA	GCGGGATCCTTACATGTTACTGATACTATTCTC	BamHI	RT-PCR / 35S::AtHB13ΔAHA
AtHB13 ΔCTR	GCGGGATCCTCATGATTCTGTTTGTTCTCTG	BamHI	35S::AtHB13ΔCTR
AtHB13 W285A W287A	GCGGATCCTCAATTGTACTGTTGCTGATCAAGCGCTGGCGCAAAACCAGA	BamHI	35S::AtHB13WxA
AtHB13 D289A	GCGGGATCCTCAATTGTACTGTTGCTGAGCAAGCCA	BamHI	35S::AtHB13D289A
AtHB23q F	TTGATGACCAGTCTGGGTTC		Quantification by RT-qPCR
AtHB23q R	GAATTGGTTCATCTGACCACTT		Quantification by RT-qPCR
AtHB23 F	GGGGGATCCATGTCTTGTAATAATAATGGCTTAGC	BamHI	35S::AtHB23
AtHB23 R	GGGCTCGAGTCATCAATTGTATTGTTGCTGGTC	XhoI	35S::AtHB23 / Control of transgene presence
amiRNA 13/23 I	GATATTCAATTGTATTGTGGCTGTCTCTCTTTTGTATTCC		35S::amiR13/23
amiRNA 13/23 II	GACAGCCACAATACAATTGAATATCAAAGAGAATCAATGA		35S::amiR13/23
amiRNA 13/23 III	GACAACCACAATACATTTGAATTTCACAGGTCGTGATATG		35S::amiR13/23
amiRNA 13/23 IV	GAAATTCAAATGTATTGTGGTTGTCTACATATATATTCCT		35S::amiR13/23
amiRNA 23 I	GATAATGTCTAATCATATGGCACTCTCTCTTTTGTATTCC		35S::amiR23
amiRNA 23 II	GAGTGCCATATGATTAGACATTATCAAAGAGAATCAATGA		35S::amiR23
amiRNA 23 III	GAGTACCATATGATTTGACATTTTCACAGGTCGTGATATG		35S::amiR23
amiRNA 23 IV	GAAAATGTCAAATCATATGGTACTCTACATATATATTCCT		35S::amiR23

35Spromoter F	TGACGCACAATCCCACTATC		Control of transgene presence
AtHB13 R	GCCGGATCCATTTCAATTGTACTGTTGCTGATC	BamHI	Control of transgene presence
athb13-2 LP	CGACCAAAATCTCAAGCAAAC		Control of transgene presence
athb13-2 RP	CGGCGCAGTTGAGATATCTAG		Control of transgene presence
T-DNA GK 08409	ATATTGACCATCATACTCATTGC		Control of transgene presence
athb13-1 LP	AGGAGTTGCTTTCAGGTAGGG		Control of transgene presence
athb13-1 RP	TATGAAATTGATGGTCTGCGG		Control of transgene presence
LB3 T-DNA Sail	TAGCATCTGAATTTCATAACCAATCTCGATACAC		Control of transgene presence
prATHB13 F	GGGGACAAGTTTGTACAAAAAAGCAGGCTTAGAATGAAGACCGTATTAGATAAGG		pAtHB13::GUS
prAtHB13 R	GGGTCTAGACTTCTTCTGTTTTGCAACAGAAGTTAG	XbaI	pAtHB13::GUS
GRP17 (At5g07530) F	GTCAAAGGCAAAGTCTAAAGGTG		Quantification by RT-qPCR
GRP17 (At5g07530) R	AGACATACCTTCATCCCCAGAC		Quantification by RT-qPCR
AtOPT8 (At5g53520) F	CTCGTTATGATCACCACTCAGG		Quantification by RT-qPCR
AtOPT8 (At5g53520) R	TGATGAGAGTGATGACAAAGAAC		Quantification by RT-qPCR
AtPTR5 (At5g01180) F	AACTCTGTCGTCGCTTCCCC		Quantification by RT-qPCR
AtPTR5 (At5g01180) R	ACAGCACTCAGTTCCAAGAATG		Quantification by RT-qPCR
SKS2 (At5g51480) F	TCAACAGGTTATAGCAGTCAATG		Quantification by RT-qPCR
SKS2 (At5g51480) R	ATAAGTGAAGTTCCAATTCGGTG		Quantification by RT-qPCR
GDSL-Like lipase (At5g03810) F	GGTGGGGTCGGGAACAATATG		Quantification by RT-qPCR
GDSL-Like lipase (At5g03810) R	GATTCGAAAAACCCATACTCGAC		Quantification by RT-qPCR
GRP (At2g15340) F	GTTATAGCCATTGCATGTCTCTC		Quantification by RT-qPCR

GRP (At2g15340) R	CTAAAACCACCAGAATTCGGAC		Quantification by RT-qPCR
CAP (At3g19690) F	GCCCACAACGAAGCCCGAAA		Quantification by RT-qPCR
CAP (At3g19690) R	CGCAGCATCTTCAGCCGACA		Quantification by RT-qPCR
F2809.220 (At3g57370) F	TAATGGCCGTAGGGCTCCTG		Quantification by RT-qPCR
F2809.220 (At3g57370) F	TTGGCAAACCACGTGGGTACT		Quantification by RT-qPCR
CYCMEE65 (At2g01280)F	GGTGGTTTGGCATGTGATTTATG		Quantification by RT-qPCR
CYCMEE65 (At2g01280)R	GAGCTTGAATTCCCAACACTCG		Quantification by RT-qPCR
CYCP3;2 (At3g60550) F	AACAATTCCAAGACACCTCTGG		Quantification by RT-qPCR
CYCP3;2 (At3g60550) R	AAAGATCTGAGTTTTGCCACCG		Quantification by RT-qPCR
CYCJ18 (At2g01905) F	CTTCAAAATCTCTGGCTGCTTC		Quantification by RT-qPCR
CYCJ18 (At2g01905) R	TTGTCACCATTTTAACCCAGGG		Quantification by RT-qPCR
CYCB1;5 (At1g34460) F	CGAGACGAAGAGGAATGCTC		Quantification by RT-qPCR
CYCB1;5 (At1g34460) R	GTGCATGTACATCTTAGGCTGA		Quantification by RT-qPCR
PLP4 (At4g37050) F	GCATCGAAATGGGGATTGATGTG		Quantification by RT-qPCR
PLP4 (At4g37050) R	TCGGAACGAAGAGCTTGAAAGAC		Quantification by RT-qPCR
PMEI (At5g62360) F	ATgCggCTCTCAACATCACATTAg		Quantification by RT-qPCR
PMEI (At5g62360) R	TCTCATggCCgAgACTTCTTTAgg		Quantification by RT-qPCR
CESA10 (At2g25540) F	ggTCTgCACTTCTTgCATCCATC		Quantification by RT-qPCR
CESA10 (At2g25540) R	ggCAgCTCACTCACCCATgAAAC		Quantification by RT-qPCR
EXP10 (At1g26770) F	AGCGAACAATAATGGCGGTTGG		Quantification by RT-qPCR
EXP10 (At1g26770) R	CTTCTCCTGCAAGGAACCCTTC		Quantification by RT-qPCR
XTH15 (At4g14130) F	ggAgACCCCAACACATCATATTCTT		Quantification by RT-qPCR

XTH15 (At4g14130) R	CACCTCTCgTggCCCAATCg		Quantification by RT-qPCR